Article:
Neal, T.J., Parnell, A.J., King, S.M. et al. (2021) Control of particle size in the self-assembly of amphiphilic statistical copolymers. Macromolecules, 54 (3). pp. 1425-1440. ISSN: 0024-9297

https://doi.org/10.1021/acs.macromol.0c02341

Macromolecules

pubs.acs.org/Macromolecules Article

Control of Particle Size in the Self-Assembly of Amphiphilic Statistical Copolymers

Thomas J. Neal, Andrew J. Parnell, Stephen M. King, Deborah L. Beattie, Martin W. Murray, Neal S. J. Williams, Simon N. Emmett, Steven P. Armes, Sebastian G. Spain,* and Oleksandr O. Mykhaylyk*

Cite This: *Macromolecules* 2021, 54, 1425−1440 Read Online

ACCESS | Metrics & More | Article Recommendations | Supporting Information

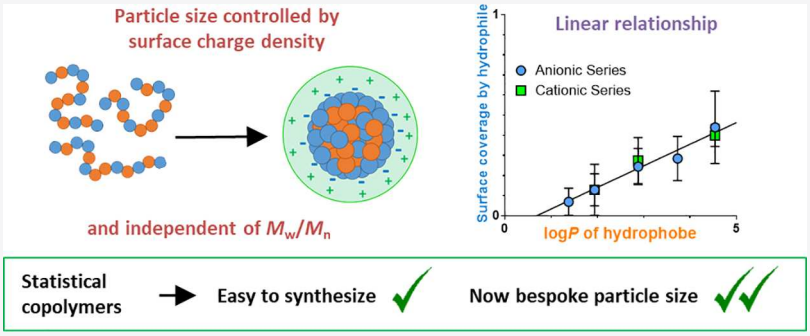

ABSTRACT: A range of amphiphilic statistical copolymers is synthesized where the hydrophilic component is either methacrylic acid (MAA) or 2-(dimethylamino)ethyl methacrylate (DMAEMA) and the hydrophobic component comprises methyl, ethyl, butyl, hexyl, or 2-ethylhexyl methacrylate, which provide a broad range of partition coefficients (log *P*). Small-angle X-ray scattering studies confirm that these amphiphilic copolymers self-assemble to form well-defined spherical nanoparticles in an aqueous solution, with more hydrophobic copolymers forming larger nanoparticles. Varying the nature of the alkyl substituent also influenced self-assembly with more hydrophobic comonomers producing larger nanoparticles at a given copolymer composition. A model based on particle surface charge density (PSC model) is used to describe the relationship between copolymer composition and nanoparticle size. This model assumes that the hydrophilic monomer is preferentially located at the particle surface and provides a good fit to all of the experimental data. More specifically, a linear relationship is observed between the surface area fraction covered by the hydrophilic comonomer required to achieve stabilization and the log *P* value for the hydrophobic comonomer. Contrast variation small-angle neutron scattering is used to study the internal structure of these nanoparticles. This technique indicates partial phase separation within the nanoparticles, with about half of the available hydrophilic comonomer repeat units being located at the surface and hydrophobic comonomer-rich cores. This information enables a refined PSC model to be developed, which indicates the same relationship between the surface area fraction of the hydrophilic comonomer and the log *P* of the hydrophobic comonomer repeat units for the anionic (MAA) and cationic (DMAEMA) comonomer systems. This study demonstrates how nanoparticle size can be readily controlled and predicted using relatively ill-defined statistical copolymers, making such systems a viable attractive alternative to diblock copolymer nanoparticles for a range of industrial applications.

INTRODUCTION

Self-assembled copolymers have applications in a wide range of diverse fields, including healthcare,[1−7] energy,[8,9] and coatings.[10−12] The assembly of diblock copolymers in solution has been studied extensively and is driven by minimization of the energetically unfavorable interactions between the solvent and the solvophobic block.[13] The morphology of diblock copolymer nano-objects depends on the relative volume fractions of solvophilic and solvophobic blocks and can be rationalized in terms of the fractional packing parameter.[14−16] For a fixed diblock composition, the nano-object dimensions depend on both the overall copolymer molecular weight and also the aggregation number, with the latter parameter depending on the processing conditions.[17,18]

In contrast to amphiphilic diblock copolymers, amphiphilic statistical copolymers (ASC) comprise hydrophilic and hydrophobic comonomers that are distributed throughout each

Received: October 15, 2020
Revised: January 5, 2021
Published: January 22, 2021

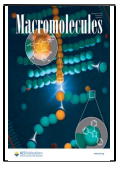

https://dx.doi.org/10.1021/acs.macromol.0c02341
Macromolecules 2021, 54, 1425−1440

Scheme 1. (a) Representative Diagram of a Statistical Copolymerization; (b) RAFT Solution Copolymerization of Either MAA or DMAEMA (*B*) with EHMA, HMA, BMA, EMA, or MMA (*A*) to Form a Range of P(*A*-*stat*-*B*) ASCs; and (c) Standard Free-Radical Copolymerization of MAA and a Hydrophobic Methacrylate Monomer[a]

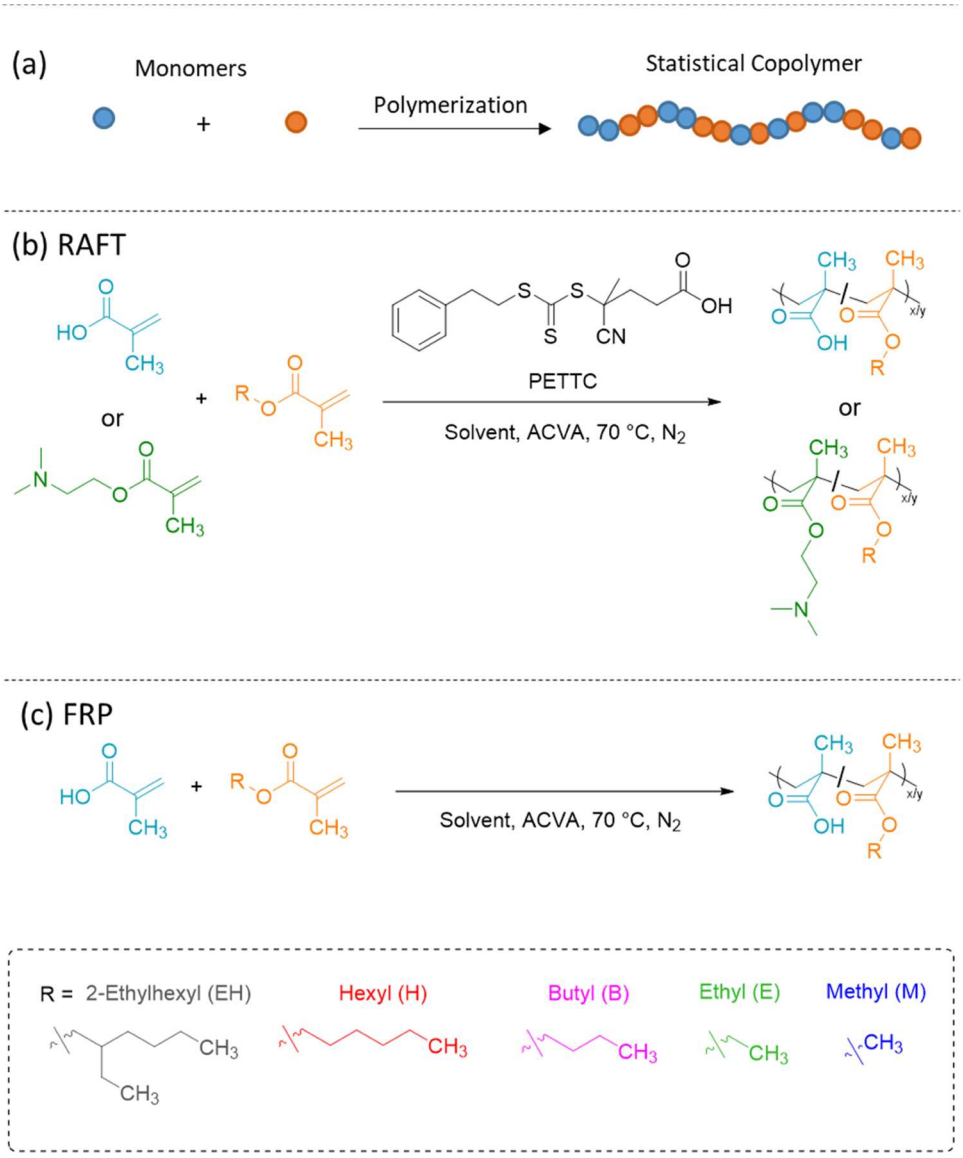

[a]Copolymerization of BMA with MAA was performed in 1,4-dioxane at 50% w/w, whereas all other copolymerizations were performed in IPA at the same concentration.

copolymer chain rather than being spatially segregated. More importantly, such copolymers are readily synthesized without using the controlled/living polymerization techniques that are required for the synthesis of diblock copolymers. As such, they are routinely prepared on an industrial scale (i.e., millions of tonnes per annum) using conventional free-radical copolymerization.[19] Like diblock copolymers, ASCs can self-assemble to form a range of copolymer morphologies, including spheres,[20−22] rods/worms,[23−25] and vesicles.[22,26] Furthermore, Liu et al. reported that statistical copolymers comprising styrene and methacrylic acid could form a remarkable "bowl-like" morphology in an aqueous solution.[27] It has also been demonstrated by Zhu and Liu that statistical copolymers of *N*-acryloyl-L-glutamic acid and *N*-dodecyl acrylamide can self-assemble to form either spheres or vesicles depending on the choice of solvent.[28] Statistical distribution of the solvophobic groups along the copolymer backbone also enables microphase separation on shorter length scales (<10 nm) than that typically achieved for block copolymers.[29] Moreover, both copolymer composition and solvophobe type can affect the domain size of the nanoparticles.[29−31] Recently, Imai et al. showed that ASCs composed of poly(ethylene glycol) methacrylate statistically copolymerized with either *n*-butyl methacrylate or *n*-dodecyl methacrylate self-assembled in an aqueous solution to form structures in which copolymer chains were self-sorted both in terms of their composition and choice of hydrophobic comonomer.[32] Matsumoto et al. found that block copolymers consisting of two different statistical blocks with a common hydrophilic poly(ethylene glycol) methacrylate component self-organize to yield nano-objects with distinct compartments.[31]

https://dx.doi.org/10.1021/acs.macromol.0c02341
Macromolecules 2021, 54, 1425−1440

Despite these advances, the rationalization and understanding of nano-object dimensions and morphology formed by ASCs has been rather limited. Sato et al. found that higher degrees of ASC polymerization lead to lower aggregation numbers of molecules assembling in nanoparticles.[33] Similarly, it was recently reported that the size of self-assembled nanoparticles formed by amphiphilic poly(butyl methacrylate-*stat*-methacrylic acid) [P(BMA-*stat*-MAA)] copolymers depends on the copolymer composition but is independent of the copolymer molecular weight.[34] To describe the observed particle size behavior, a particle surface charge density (PSC) model based on the ionized surface charge density arising from the anionic MAA units was proposed.[34] Herein, this model is generalized for charged nanoparticles formed by various ASC systems comprising either positively or negatively charged ionic comonomers. More specifically, this PSC model has been validated for a series of MAA-based statistical copolymers comprising a range of hydrophobic alkyl methacrylate comonomers synthesized using either reversible addition−fragmentation chain transfer (RAFT) polymerization or conventional free-radical polymerization (FRP) (Scheme 1). These anionic ASCs are complemented by an analogous series of cationic ASCs prepared using 2-(dimethylamino)ethyl methacrylate (DMAEMA) as the hydrophilic comonomer. Importantly, it is demonstrated that (i) the particle size is correlated with the partition coefficient ($\log P$) of the hydrophobic comonomer and (ii) this model can be used to predict the nanoparticle size for a given hydrophobic comonomer and target copolymer composition.

EXPERIMENTAL SECTION

Materials. Methyl methacrylate (MMA, 99%), ethyl methacrylate (EMA, 99%), *n*-butyl methacrylate (BMA, 99%), *n*-hexyl methacrylate (HMA, 99%), DMAEMA (99%), and MAA (99.5%) were purchased from Sigma-Aldrich (Gillingham, U.K.) and were passed through a basic alumina column to remove inhibitor prior to polymerization. 2-Ethylhexyl methacrylate (EHMA, 98%) was purchased from Alfa Aesar (Heysham, U.K.), and its inhibitor was removed using an alumina column. Isopropanol (IPA, 99.9%), triethanolamine (TEA, 99%), 4,4′-azobis(4-cyanovaleric acid) (ACVA), 1,4-dioxane (99.5%), trimethylsilyldiazomethane solution (2.0 M in diethyl ether), benzyl bromide (BzBr, 98%), and deuterated acetone were purchased from Sigma-Aldrich. Deuterated chloroform ($CDCl_3$) and deuterated dimethyl sulfoxide (DMSO-d_6) for NMR spectroscopy measurements were purchased from VWR (Lutterworth, U.K.). Deionized water was obtained using an Elgastat Option 3A water purifier (Elga, High Wycombe, U.K.). 4-Cyano-4-(2-phenylethanesulfanylthiocarbonyl)-sulfanylpentanoic acid (PETTC) used for RAFT polymerization was prepared and purified in-house, as reported previously.[35] Unless stated otherwise, all materials were used as received.

^{1}H NMR Spectroscopy. ^{1}H NMR spectra were recorded in either DMSO-d_6 or $CDCl_3$ using a Bruker AV1-400 or AV3HD-400 MHz spectrometer. These spectra were analyzed using Bruker Topspin 3.5pl7 software and chemical shifts are reported relative to a residual solvent peak. Copolymer compositions were calculated using ^{1}H NMR spectra of alkylated copolymers where methacrylic acid repeat units were alkylated prior to the measurements using either trimethylsilyldiazomethane to form methyl methacrylate residues[36] or BzBr to form benzyl methacrylate residues. In the former reaction, excess trimethylsilyldiazomethane was added dropwise to a 5% w/w copolymer solution in THF (5 mL) with a few drops of methanol (approx. 0.1 mL) until the solution turned a persistent yellow color. The reaction solution was stirred overnight allowing all solvent to evaporate leaving a residue of methylated copolymer. The latter reaction was performed at 5% w/w in DMF with $CsCO_3$ being added to deprotonate the methacrylic acid repeat units, followed by BzBr addition. This alkylation reaction was allowed to proceed for 24 h, then the solvent was removed under vacuum and the derivatized copolymer product was purified by washing with water.

Gel Permeation Chromatography (GPC). Molecular weight distributions were assessed by GPC in THF containing 0.025% w/v butyl hydroxytoluene (BHT) and either 4% v/v acetic acid or 1% v/v triethylamine. The MAA-based copolymers were analyzed using the acidic eluent, whereas DMAEMA-based copolymers were analyzed using the basic eluent. Measurements were performed at a flow rate of 1.0 mL min^{-1} using an Agilent PL-GPC50-integrated GPC system equipped with a refractive index detector. Separations were carried out using a pair of PLgel Mixed-C columns (7.8 mm internal diameter, 300 mm length, and 5 μm bead size) equipped with a PLgel guard column (7.8 mm, 50 mm, and 5 μm). Calibration was achieved using a set of 10 low-dispersity poly(methyl methacrylate) (PMMA) standards (Agilent, U.K.) with peak molecular weight values ranging from 550 to 1 568 000 Da.

Small-Angle X-ray Scattering (SAXS). SAXS patterns were recorded using laboratory SAXS instruments [either a Bruker AXS Nanostar equipped with a two-dimensional (2D) Hi-STAR multiwire gas detector, and modified with a Xenocs GeniX 3D microfocus X-ray source (Cu Kα radiation, wavelength λ = 1.54 Å) and motorized collimating scatterless slits or a Xeuss 2.0 laboratory beamline (Xenocs, Grenoble, France) equipped with a 2D Pilatus 1M pixel detector (Dectris, Baden-Daettwil, Switzerland) and a MetalJet X-ray source (Ga Kα radiation, λ = 1.34 Å; Excillum, Kista, Sweden)]. Samples were run in either an open top- or a sealed flow-through borosilicate glass capillary (Capillary Tube Supplies Ltd, Cornwall, U.K.) of 2 mm diameter. Patterns were collected over a scattering vector range of 0.008 Å^{-1} < q < 0.16 Å^{-1}, where $q = \frac{4\pi}{\lambda}\sin\theta$ and θ is half the scattering angle. 2D X-ray scattering patterns were reduced to one-dimensional curves using the Nika SAS macro (version 1.74) for Igor Pro[37] or software supplied by the SAXS instrument manufacturers. Background subtraction and further data analysis were performed using Irena SAS macro (version 2.61) for Igor Pro.[38] The scattering of pure water was used for the absolute intensity calibration of the SAXS patterns.

Small-Angle Neutron Scattering (SANS). SANS measurements were performed on the LOQ diffractometer at the ISIS Spallation Neutron Source (Didcot, U.K.)[39] using the contrast variation technique. The sample-to-detector distance was 4.1 m and the beam diameter was 10 mm. The solutions were pipetted into either 1 or 2 mm path length PTFE-stoppered quartz cuvettes (Hellma UK) depending on the solvent (either H_2O or H_2O/D_2O mixtures, respectively). Cuvettes were mounted on a computer-controlled sample changer maintained at a fixed temperature of 25 °C. Scattering patterns were recorded using an Ordela 2D multiwire gas detector, and each data set was corrected for the incident neutron wavelength distribution, the detector efficiency and spatial linearity, and the measured transmission and cuvette path length, before being radially averaged and converted to coherent elastic differential scattering cross-section per unit sample volume data ($\partial\sum/\partial\Omega$) as a function of q using the Mantid software framework.[40] In the following text, $\partial\sum/\partial\Omega$ is referred to as the intensity, I. A partially deuterated polymer blend standard of known molecular weight was used to scale the reduced SANS data to an absolute intensity scale in accordance with well-established protocols.[41] Background subtraction and some data analysis was performed using the Irena SAS macro for Igor Pro.[38]

Transmission Electron Microscopy (TEM). TEM imaging was performed on 0.1% w/w copolymer dispersions. Copper/palladium TEM grids (Agar Scientific, U.K.) surface-coated in-house by a thin film of amorphous carbon were used as sample substrates. Before a sample deposition, the substrate surface was treated by plasma glow discharge for 30 s to make it hydrophilic. A copolymer solution (0.1% w/w, 9 μL) was pipetted onto a freshly glow discharged grid for 20 s and then blotted to remove the excess using filter paper. These were negatively stained using an aqueous solution of uranyl formate (0.75% w/w, 9 μL). The sample-loaded grid was exposed to the stain for 30 s before removing the excess by blotting. Grids were dried using a

https://dx.doi.org/10.1021/acs.macromol.0c02341
Macromolecules 2021, 54, 1425−1440

Table 1. Summary of Experimental Data Obtained for P(*A-stat-B*) Copolymers, Where *synth* Denotes the Polymerization Method Used, (*A*:*B*) is the Molar Ratio of *A* and *B* Comonomers, M_n, M_w, and M_w/M_n are the Number-Average Molecular Weight, Weight-Average Molecular Weight, and Copolymer Dispersity Determined from GPC Analysis, Respectively (See Figure S5 for Representative GPC Traces)

				composition (*A*:*B*)[a]		GPC[b]		
synth.	*B*	*A*	copolymer name	targeted	actual	M_n, kDa	M_w, kDa	M_w/M_n
RAFT	MAA (M)	MMA (M)	MM_{6040}	60:40	62:38	21.5	30.4	1.42
			MM_{7030}	70:30	71:29	28.0	39.8	1.42
			MM_{8020}	80:20	81:19	25.6	31.0	1.21
			MM_{8812}	88:12	88:12	27.3	32.8	1.19
			MM_{9010}	90:10	90:10	23.6	29.6	1.25
			MM_{9505}	95:05	95:05	23.1	28.7	1.24
			MM_{9802}	98:02	97:03	21.7	26.8	1.24
		EMA (E)	EM_{6040}	60:40	60:40	33.5	44.4	1.33
			EM_{7030}	70:30	70:30	33.0	42.8	1.30
			EM_{8020}	80:20	80:20	27.3	33.2	1.22
			EM_{8119}	81:19	81:19	30.7	38.3	1.25
			EM_{8416}	84:16	84:16	22.6	28.8	1.27
			EM_{8614}	86:14	86:14	24.1	30.1	1.25
			EM_{9010}	90:10	90:10	26.2	32.5	1.24
		BMA (B)	BM_{6040}	60:40	61:39	37.9	44.6	1.18
			BM_{7030}	70:30	71:29	36.4	45.4	1.25
			BM_{7525}	75:25	76:24	35.2	44.9	1.28
			BM_{8020}	80:20	80:20	39.0	48.8	1.25
			BM_{8515}	85:15	86:14	33.6	40.6	1.21
			BM_{9010}	90:10	90:10	27.1	30.1	1.11
		HMA (H)	HM_{5050}	50:50	49:51	28.6	34.4	1.20
			HM_{6040}	60:40	61:39	28.3	33.6	1.19
			HM_{7030}	70:30	68:32	31.1	37.2	1.19
			HM_{8020}	80:20	76:24	33.5	40.1	1.20
		EHMA (EH)	EHM_{3070}	30:70	31:69	34.7	57.9	1.66
			EHM_{4060}	40:60	41:59	37.0	48.8	1.31
			EHM_{5050}	50:50	49:51	37.5	47.3	1.26
			EHM_{6040}	60:40	61:39	40.8	54.7	1.34
			EHM_{7030}	70:30	71:29	25.5	32.6	1.28
			EHM_{8020}	80:20	80:20	29.8	33.0	1.11
	DMAEMA (D)	EMA (E)	ED_{8515}	85:15	85:15	22.8	27.4	1.20
			ED_{9010}	90:10	90:10	22.5	27.2	1.21
			ED_{9307}	93:07	93:07	23.1	27.7	1.20
			ED_{9505}	95:05	95:05	23.4	28.1	1.20
		BMA (B)	BD_{6040}	60:40	61:39	26.9	34.4	1.28
			BD_{7030}	70:30	68:32	28.7	36.4	1.27
			BD_{7525}	75:25	73:27	28.9	36.4	1.26
			BD_{8020}	80:20	78:22	29.4	35.6	1.21
			BD_{8515}	85:15	84:16	26.0	32.0	1.23
		EHMA (EH)	EHD_{5050}	50:50	51:49	31.1	38.6	1.31
			EHD_{6040}	60:40	61:39	24.5	33.0	1.35
			EHD_{7030}	70:30	71:29	22.2	28.2	1.27
FRP	MAA (M)	BMA (B)	$BM_{7030(FRP)}$	70:30	69:31	13.2	23.9	1.81
			$BM_{8020(FRP)}$	80:20	78:22	16.5	31.2	1.89
			$BM_{9010(FRP)}$	90:10	88:12	11.5	21.2	1.85

[a]Copolymer compositions were determined by ^{1}H NMR spectroscopy analysis of the respective alkylated copolymers. [b]The GPC measurements were performed using THF eluent containing 0.025% w/v butyl hydroxytoluene (BHT) and either 4% v/v acetic acid or 1% v/v triethylamine against PMMA standards.

vacuum hose. Imaging was performed at 120 kV using a FEI Tecnai G2 Spirit TEM instrument equipped with a Gatan 1kMS600CW CCD camera.

Synthesis of Statistical Copolymers. The copolymerization protocol for producing a P(*A-stat-B*) amphiphilic statistical copolymer, where *A* is hydrophobic comonomer and *B* is hydrophilic comonomer, is illustrated here for all cases by a synthesis of P(EMA-*stat*-MAA) with EMA to MAA molar ratio of 80:20 (EH_{8020}, see Table 1).

EMA (monomer *A*, 1.26 g, 11.1 mmol), MAA (monomer *B*, 0.238 g, 2.76 mmol), ACVA (4.70 mg, 0.017 mmol), and PETTC (17.1 mg, 0.050 mmol) were mixed in IPA (1.52 g) [1,4-dioxane was used instead of IPA for the P(BMA-*stat*-MAA) series] creating a 50% w/w monomer solution and placed in an ice bath to cool. The mixture was degassed with N_2 for 20 min and then heated to 70 °C to initiate the

https://dx.doi.org/10.1021/acs.macromol.0c02341
Macromolecules 2021, 54, 1425−1440

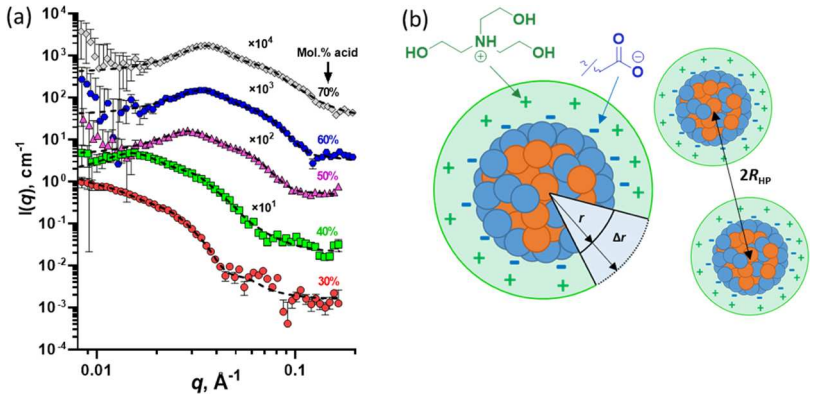

Figure 1. (a) SAXS patterns recorded for 1.0% w/w aqueous dispersions of P(EHMA-*stat*-MAA) copolymer nanoparticles (symbols) using a Bruker AXS Nanostar instrument. A core−shell form factor (dotted lines; eqs S8−S11) was fitted to determine the mean size of nanoparticles formed by copolymers comprising 30, 40, 50, 60, or 70 mol % MAA. Patterns are shifted upwards by arbitrary numerical factors (indicated on the plot) to aid clarity. (b) Schematic cartoon of the core−shell model used to fit the SAXS patterns accounting for the hydrated shell of TEA cations surrounding each nanoparticle, where r is the nanoparticle radius, Δr is the thickness of the cation shell, and $2R_{HP}$ is the interparticle distance determined using the Hayter−Penfold approximation for the charged sphere structure factor. A protonated TEA molecule (cation, green) and an ionized MAA unit in its anionic carboxylate form (anion, blue) are also shown.

reaction. The copolymerization was allowed to proceed for 24 h before quenching by cooling to ambient temperature with concomitant exposure to air. The product was purified by precipitation from petroleum ether and then dried in a 30 °C vacuum oven overnight to give a pale-yellow powder.

RESULTS AND DISCUSSION

Synthesis of Amphiphilic Statistical Copolymers. A series of methacrylic P(*A*-*stat*-*B*) ASCs was synthesized (Scheme 1a) in which the hydrophobic comonomer and the overall copolymer composition were systematically varied. Either anionic (MAA) or cationic (DMAEMA) monomers were used as the hydrophilic component (*B*) to examine whether the polarity of the surface charge had any influence. Five different alkyl methacrylates (e.g., MMA, EMA, BMA, HMA, or EHMA) were used in turn as the hydrophobic comonomer (*A*) to target a wide range of log *P* values, which is a commonly used parameter to quantify hydrophobicity/hydrophilicity (see Table S1).[42]

P(*A*-*stat*-*B*) copolymers were synthesized via RAFT solution copolymerization (Scheme 1) targeting a consistent overall molecular weight (ca. 30 kDa) while varying the copolymer composition. With the exception of the P(BMA-*stat*-MAA) copolymer series, all of the RAFT-synthesized copolymers were prepared in IPA at 50% w/w. Kinetic studies of such batch copolymerization suggested that the instantaneous rate of consumption of the two comonomers was comparable throughout the course of the reaction (Figures S1 and S2). Thus, an approximately statistical distribution of the hydrophobic and hydrophilic comonomers within each copolymer chain can be assumed, and the final copolymer composition is close to that targeted. Recently, it was reported that copolymerization of BMA and MAA at 20% w/w in IPA produces somewhat "blocky" copolymer chains with an undesirable BMA-rich terminus caused by a significant reduction in the rate of consumption of the acidic comonomer toward the end of the reaction.[34] To avoid this problem, IPA was replaced with 1,4-dioxane while performing the copolymerization at the same 50% w/w concentration; this strategy resulted in both comonomers being consumed at comparable rates throughout the copolymerization (Figure S1c).

Each series forms stable colloidal dispersions of copolymer nanoparticles at different acid/amine contents depending on the nature of the hydrophobic alkyl methacrylate comonomer. For example, P(EHMA-*stat*-MAA) copolymers require a higher acid content to produce stable colloidal dispersions compared to P(MMA-*stat*-MAA) because EHMA is significantly more hydrophobic than MMA (Table 1).

Copolymer compositions were determined by ^{1}H NMR spectroscopy (after exhaustive alkylation in the case of the MAA-based copolymers; see Figures S3 and S4). As suggested by the kinetic analysis, the final copolymer compositions were always in good agreement with the initial comonomer feed ratios (Table 1). A consistent molecular weight was targeted for each copolymer to minimize the number of variables for a given copolymer type and composition. Copolymers within each comonomer series exhibited similar M_w values by GPC, but some discrepancies were observed between series (Table 1). Molecular weight data are expressed relative to PMMA calibration standards; thus, systematic differences between copolymer series are expected as each of the different hydrophobic components and compositions will result in different hydrodynamic volumes for a given chain length compared to the PMMA standards in the GPC eluent (THF).[43] Where the MAA weight fraction was high (e.g., MM_{6040}, EHM_{3070}), increased M_w/M_n was observed (Table 1), which is attributed to reduced solubility in the GPC eluent leading some aggregation. Previous research suggests little or no correlation between copolymer molecular weight and nanoparticle size for relatively high aggregation numbers.[33,34] Thus, minor inconsistencies between molecular weights are unlikely to adversely affect the particle size formed within this regime. However, for relatively low aggregation numbers, when copolymer interactions are mainly intramolecular in nature, the copolymer molecular weight may affect the particle size. In particular, this aspect should be taken into account when considering the formation of single-chain nanoparticles (for which the aggregation number is one).

One significant advantage of statistical copolymers is that they can be readily prepared by free-radical polymerization (FRP), which is a relatively simple and inexpensive process. Since FRP inevitably produces broad molecular weight

https://dx.doi.org/10.1021/acs.macromol.0c02341
Macromolecules 2021, 54, 1425−1440

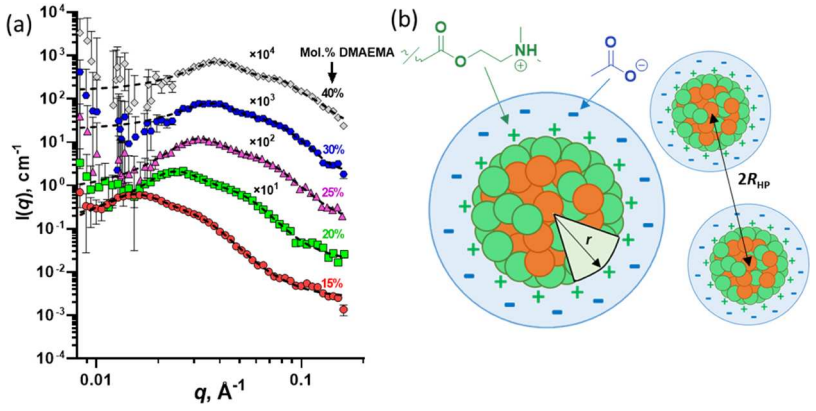

Figure 2. (a) SAXS patterns recorded using a Bruker AXS Nanostar instrument for 1.0% w/w aqueous dispersions of P(BMA-*stat*-DMAEMA) copolymer nanoparticles (symbols) fitted using a sphere model (eq S7) (dotted lines) to calculate the mean nanoparticle radius for copolymers comprising 15, 20, 25, 30, or 40 mol % DMAEMA. Some patterns are shifted upwards by arbitrary numerical factors to aid clarity. (b) Schematic cartoon showing how the anions surround the cationic nanoparticles to form a hydrated anionic shell, where r is the nanoparticle radius and $2R_{HP}$ is the interparticle distance determined using the Hayter−Penfold approximation for the charged sphere structure factor. A protonated DMAEMA unit (cation, green) and an ionized acetate (anionic, blue) are also shown. Since the SLD of acetic acid is close to that of water and the SLD contrast between the copolymer and water is high, these SAXS measurements are not sensitive to the anionic shell. Thus, SAXS patterns are satisfactorily fitted using a simplified sphere form factor (eq S7) rather than the more complicated core−shell form factor required for anionic copolymer dispersions (Figure 1).

distributions, a small series of P(BMA-*stat*-MAA) copolymers (Scheme 1c) comprising 10−30 mol % MAA was prepared using FRP (M_w/M_n > 1.85) instead of RAFT polymerization (M_w/M_n < 1.50) to assess the effect of the polymerization method and copolymer dispersity on the self-assembly behavior, see Table 1.

Self-Assembly of Amphiphilic Statistical Copolymers. Aqueous dispersions of ASC nanoparticles were obtained using a solvent-switch method. Each copolymer was initially dissolved at 50% w/w in a good solvent (IPA) and then diluted slowly using water. Dilution of MAA-based copolymers was performed in the presence of triethanolamine (TEA; 1.1 equiv relative to MAA residues). This organic base deprotonates the MAA comonomer units, thereby producing the anionic surface charge required to stabilize the copolymer nanoparticles. Conversely, dilution of the DMAEMA-based copolymers was performed in the presence of sufficient acetic acid to protonate the pendent tertiary amine groups and hence confer a cationic surface charge. In each case, slow addition of water drives *in situ* intramolecular and intermolecular self-assembly of the strongly amphiphilic copolymer chains. The hydrophobic alkyl methacrylate repeat units self-assemble to form nanoparticles that are stabilized by the charged hydrophilic groups. Copolymer dispersions were diluted to 1.0% w/w to (i) minimize the volume fraction of the remaining water-miscible good solvent (IPA) and (ii) reduce the interparticle interactions that are present at higher copolymer concentrations. The pH of the 1.0% w/w anionic dispersions was measured to be around 8, which is much higher than the pK_a of MAA (pK_a ∼ 4−5)[44] providing evidence that all (99.9%) of the MAA units are deprotonated. Likewise, the pH of the cationic dispersions were approximately 4, which is much lower than the pK_a of DMAEMA (pK_a ∼ 7)[45] verifying that the all (99.9%) DMAEMA units are protonated.

SAXS was utilized to investigate the copolymer morphology of the colloidal dispersions. SAXS patterns recorded for 1.0% w/w dispersions of the MAA-based copolymers indicated the formation of spherical nanoparticles (Figures 1a and S6), which is consistent with prior studies of closely related copolymers.[34] Additionally, well-defined spherical particles were observed by TEM (Figure S7) further validating the self-assembly of these copolymers. However, TEM is not an ideal structural analysis method for this study as the particle dimensions are often below the reliable resolution of the microscope. Moreover, the particle shape might be distorted during the sample preparation. Especially, when the glass transition temperatures (T_g) of both PHMA and PEHMA are below room temperature and particles formed by the associated copolymers will not retain the structure once dried. Instead, SAXS was chosen as particles can be assessed in their dispersed state *in situ* and nanoparticle dimensions can be measured with a high degree of accuracy. In addition, SAXS is a much more statistically reliable method in a comparison with microscopy techniques as scattering data are collected from a relatively large sample volume and, therefore, are averaged over millions of particles. The scattering patterns can be satisfactorily fitted using an intensity equation (see the Supporting Information, eqs S1, S34, or S35) incorporating a spherical core−shell form factor (eqs S8−S11), which accounts for a "shell" of cations (protonated TEA molecules) that are associated with the anionic nanoparticles (Figure 1b). This structural feature cannot be ignored in the scattering analysis because the scattering length density (SLD) of TEA is substantially greater than that of water (ξ_{TEA} = 10.54 × 10^{10} cm^{-2} and ξ_{water} = 9.42 × 10^{10} cm^{-2}), which produces significant contrast. The mean thickness of the TEA cationic shell (Δr, Figure 1b) is fixed at 6 Å during the fitting. This value corresponds to the approximate length of a single TEA unit within the shell (eq S12). Furthermore, the SLD of this cationic TEA shell is highly dependent on the volume fraction of water molecules within it. Following the earlier PSC model,[34] it was assumed that all of the MAA repeat units are located at the surface of the nanoparticles (i.e., k = 1, where k is the fraction of surface-confined MAA units relative to all available MAA units). Further, it was assumed that every surface-confined anionic MAA unit has an associated protonated TEA cation. Based on these assumptions, the relative volumes of TEA and water within the cationic shell can

https://dx.doi.org/10.1021/acs.macromol.0c02341
Macromolecules 2021, 54, 1425−1440

be estimated for the core−shell model (eqs S13−S16), enabling the shell SLD to be calculated from the nanoparticle size when fitting the SAXS patterns. According to prior studies of a closely related ASC system, the solvent concentration within the nanoparticle cores is close to zero (about a few vol %).[34] Thus, to simplify the SAXS model, it is assumed in the SAXS analysis that the solvent volume fraction in the particle core, x_{sol}, equals zero.

A high q plateau ($q > 0.1$ Å^{-1}) is observed in the scattering patterns recorded for most of the copolymer dispersions (Figures 1a, 2a, S6, and S9). This structural feature has been observed for similar ASC systems[34,46] and is possibly associated with electron density fluctuations within the nanoparticles owing to the statistical distribution of comonomer repeat units and/or thermal motion of the copolymer chains. A linear background intensity was incorporated into the intensity equation to account for this feature (eq S34). In some cases, there is an upturn at low q ($q < 0.015$ Å^{-1}) caused by nanoparticle clusters formed as a result of their strong charges fixing them in space with respect to each other so they appear as a larger coherent structure. This feature requires a power law function to be incorporated into the intensity equation (eq S35). Fitting the modified intensity equation (either eqs S34 or S35) to the SAXS patterns enabled calculation of the mean nanoparticle radius (R, Table 2). However, similar results were obtained if the low q upturn intensity region was excluded from the analysis and each SAXS pattern was fitted with the unmodified intensity equation (eq S1).

Despite the relatively low copolymer concentration used for these measurements, each SAXS pattern exhibits a structure peak at low q (0.01 Å^{-1} < q < 0.05 Å^{-1}), indicating interactions between neighboring particles (Figures 1a and S6). This phenomenon was observed in previous work[34] and is well known in dispersions of charged copolymer nanoparticles in aqueous media,[47] where the interaction distance is controlled by the copolymer concentration, the nanoparticle surface charge, and the dielectric constant of the solvent.[35,36] Accordingly, the Hayter−Penfold approximation for the charged sphere structure factor[48] (eq S33) was incorporated into the intensity equation (eqs S1, S34, or S35) to describe the particle interactions. This structure factor includes the effective radius equivalent to half of the mean interparticle distance from the center of one particle to the center of another (R_{HP}), the effective volume fraction (f_{HP}), the ionic strength of the solvent (M), the absolute temperature (T), and the solvent dielectric constant (ε) and the particle charge expressed in electrons (Q). However, the structure factor function is mainly used in this study as an analytical expression for the scattering analysis, and it is shown that the obtained form factor results (in particular, the particle radius) are virtually independent of the structure factor used [i.e., Hayter−Penfold or a hard-sphere structure factor solved with the Percus−Yevick closure relation[49,50] (commonly used in scattering models for counting an effect of particle interactions)] within the intensity equation for a wide range of copolymer dispersions (Table S2). SAXS analysis indicates that larger nanoparticles are always obtained as the MAA content is reduced for all five series of copolymer compositions, regardless of the type of hydrophobic comonomer (Table 2). For example, the particle size increases from 37 to 105 Å in the EHM series as the acid content is reduced from 70 to 30 mol %, while the particle size increases from 20 to 68 Å in the EM series as the acid content is lowered from 20 to 10 mol %. This finding is consistent with data obtained earlier for closely related systems.[34] Furthermore, an approximate mean aggregation number (N_{agg}) can be calculated by dividing the mean volume of a spherical nanoparticle by the volume occupied by a single copolymer chain (eq S6). Since the molecular weight and thus the volume occupied are similar for all of the copolymers, N_{agg} increases for larger particles (Table 2). Moreover, for an aggregation number of one, the nanoparticle volume is simply equal to that of an individual copolymer chain. The finding that the size of the dispersion is fundamentally determined by the copolymer acid (solvophilic component) content and is independent of the copolymer molecular weight[34] offers very simple design rules for controlling the size of spherical particles

Table 2. Summary of Structural Characteristics Obtained from SAXS Analysis of 1.0% w/w Dispersions of Anionic P(*A*-*stat*-MAA) Amphiphilic Statistical Copolymers (Where *A* Denotes MMA, EMA, BMA, HMA, or EHMA): the Mean Particle Radius (R) and Its Corresponding Standard Deviation (σ_R), the Mean Aggregation Number (N_{agg}) as Calculated Using eq S6 and Rounded to the Nearest Integer, and the Spheroidal Particle Aspect Ratio (α)

	form factor parameters			
copolymer	R (Å)	σ_R (Å)	N_{agg}	α
MM_{6040}	13	1	1[a,b]	3.96
MM_{7030}	13	1	1[a,b]	3.95
MM_{8020}	12	9	1[b]	1
MM_{8812}	19	14	1[b]	1
MM_{9010}	24	20	2	1
MM_{9505}	40	20	7	1
MM_{9802}	87	19	71	1
EM_{6040}	15	1	1[a,b]	3.18
EM_{7030}	14	8	1[b]	1
EM_{8020}	20	11	1[b]	1
EM_{8119}	28	13	2	1
EM_{8416}	34	11	4	1
EM_{8614}	39	12	6	1
EM_{9010}	68	21	30	1
BM_{6040}	26	6	2	1
BM_{7030}	35	7	4	1
BM_{7525}	51	10	12	1
BM_{8020}	49	11	11	1
BM_{8515}	78	13	43	1
BM_{9010}[c]				
HM_{5050}	26	5	2	1
HM_{6040}	35	6	4	1
HM_{7030}	48	9	10	1
HM_{8020}	72	13	32	1
EHM_{3070}	37	10	5	1
EHM_{4060}	47	13	9	1
EHM_{5050}	58	18	27	1
EHM_{6040}	88	23	58	1
EHM_{7030}	105	20	97	1
EHM_{8020}[c]				
$BM_{7030(FRP)}$	35	13	5	1
$BM_{8020(FRP)}$	66	16	25	1
$BM_{9010(FRP)}$	137	33	281	1

[a]Fitted using a spheroid model for anisotropic particles with an aspect ratio greater than unity. [b]Assigned to single-chain nanoparticles, although their N_{agg} is not exactly one. [c]These copolymer compositions did not form stable colloidal dispersions when diluted with water.

https://dx.doi.org/10.1021/acs.macromol.0c02341
Macromolecules 2021, 54, 1425−1440

formed by statistical copolymers. These design rules can also be considered substantially simpler than the established relationships for diblock copolymer particle size based on scaling factors[13,51,52] and packing parameters.[14,53]

A stabilization limit was observed within the BMA and EHMA series, whereby the BM_{9010} and EHM_{8020} copolymers form macroscopic precipitates rather than colloidally stable nanoparticles (Table 2 and Figure S8). Presumably, the acid content of such copolymers is insufficient to confer colloidal stability. This suggests that the nanoparticle formation is confined to a finite range of copolymer compositions, whereby the surface charge density is sufficient to ensure the nanoparticle stabilization.

In the MMA and EMA copolymer series (abbreviated to MM and EM, respectively), SAXS analysis indicates that N_{agg} becomes one at higher MAA contents (Table 2). This means that the copolymer chains no longer self-assemble via intermolecular hydrophobic interactions but instead form single-chain nanoparticles (SCNP) or self-folded chains through intramolecular hydrophobic interactions.[54−58] The critical acid content at which SCNPs are formed depends on the alkyl methacrylate comonomer. Thus, SCNPs are formed at (or above) 12 mol % MAA for the MM series, whereas the EMA series requires an acid content of at least 20 mol %. However, the BMA, HMA, and the EHMA series do not form SCNPs within the compositional range studied herein (Table 2), presumably owing to the greater hydrophobic character conferred by the larger alkyl groups.

When SCNPs are formed, SAXS analysis indicates that the particles become anisotropic. In this case, satisfactory data fits to the scattering patterns could only be obtained using a spheroidal form factor (eqs S2−S5) that incorporates an aspect ratio parameter for elongated (ellipsoidal) nanoparticles (Figure S12). This is because higher acid contents lead to more hydrophilic copolymer chains that eventually become molecularly dissolved in aqueous media. Moreover, it is well known that poly(methacrylic acid) forms either an extended structure in its highly ionized form or a relatively compact, globular structure in its neutral form.[59−62] Thus, given that these MAA-rich copolymers are dispersed at around pH 8, such elongated structures are consistent with the behavior observed for highly ionized poly(methacrylic acid).[59−62] Furthermore, this nanoparticle anisotropy is consistent with studies performed by Stals et al. on hydrogen-bonded SCNPs, which fold to produce asymmetric structures.[63] Like the majority of the anionic nanoparticles (Table 2), SAXS analysis of cationic P(*A*-*stat*-DMAEMA) ASC systems indicate the formation of spherical nanoparticles (Figures 2 and S10). However, in this case, the hydrated cationic shell should have an SLD similar to the background solvent ($\xi_{acid} = 9.32 \times 10^{10}$ cm^{-2} and $\xi_{water} = 9.42 \times 10^{10}$ cm^{-2}) and the copolymers have relatively high SLDs compared to water, so such SAXS measurements should not be particularly sensitive to the ionic shell. Thus, the SAXS patterns could be satisfactorily fitted using a simplified sphere form factor (eq S7) that does not account for the hydrated shell of counterions, rather than a core−shell model. The sphere model is simply described by the nanoparticle radius (r) corresponding to the core where the additional shell is ignored (Figure 2b).

Like the anionic nanoparticles, a structure factor peak is observed in the SAXS patterns recorded for the cationic nanoparticles (Figures 2a and S10). This feature indicates that there is a relatively strong interaction between neighboring nanoparticles. As before, the Hayter−Penfold structure factor (eq S33) was incorporated into the intensity function (eqs S1, S34, or S35) to account for this interaction. Structural analysis of all three copolymer series indicates that larger nanoparticles are always obtained as the DMAEMA content is reduced, regardless of the type of hydrophobic comonomer (Table 3);

Table 3. Summary of the Structural Characteristics of 1.0% w/w Aqueous Dispersions of P(*A*-*stat*-DMAEMA) Amphiphilic Statistical Copolymers (Where *A* Denotes EMA, BMA, or EHMA) Obtained from SAXS Analysis: the Mean Particle Radius (R) and its Corresponding Standard Deviation (σ_R), and the Mean Aggregation Number (N_{agg}) Calculated Using Eq S6, and Rounded to the Nearest Integer

	form factor		
copolymer	R (Å)	σ_R (Å)	N_{agg}
ED_{8515}	26	10	2
ED_{9010}	36	20	4
ED_{9307}	43	21	7
ED_{9505}	53	21	13
BD_{6040}	25	7	1[a]
BD_{7030}	31	3	3
BD_{7525}	34	4	3
BD_{8020}	43	9	7
BD_{8515}	60	31	19
EHD_{5050}	37	5	4
EHD_{6040}	44	3	8
EHD_{7030}	62	2	21

[a]Assigned to single-chain nanoparticles, although their N_{agg} is not exactly one.

this finding is fully consistent with the SAXS data obtained for the P(*A*-*stat*-MAA) copolymer series (Table 2). Moreover, this result further validates the conclusion that the size of the particles formed by an amphiphilic statistical copolymer can be controlled simply by the solvophobic component content.

SAXS analysis indicates that most of the amphiphilic copolymers self-assemble to form spherical nanoparticles when using the solvent-switch method regardless of the polarity of the surface charge conferred by the hydrophilic comonomer. Moreover, the particle size is strongly dependent on both the copolymer composition and also on the nature of the alkyl methacrylate comonomer. Relatively hydrophobic copolymers form macroscopic precipitates, rather than stable colloidal dispersions. Furthermore, relatively hydrophilic copolymers form distinctly anisotropic single-chain nanoparticles similar to that expected for highly ionized homopolymers.

Relationship between Nanoparticle Size and Copolymer Composition. SAXS analysis has shown that the nanoparticle size is strongly dependent on the hydrophilic comonomer content of these amphiphilic statistical copolymers (Tables 2 and 3). This is consistent with the previously proposed PSC model.[34] This simple model assumes (i) perfectly spherical particles, (ii) a constant surface charge density across a copolymer series regardless of the copolymer composition, and (iii) that there is no solvent present within the nanoparticle (i.e., $x_{sol} = 0$). In this prior study, it was found that a critical fractional surface coverage ($SA_{frac.}$) by anionic (B) units is required for colloidal stability.

https://dx.doi.org/10.1021/acs.macromol.0c02341
Macromolecules 2021, 54, 1425−1440

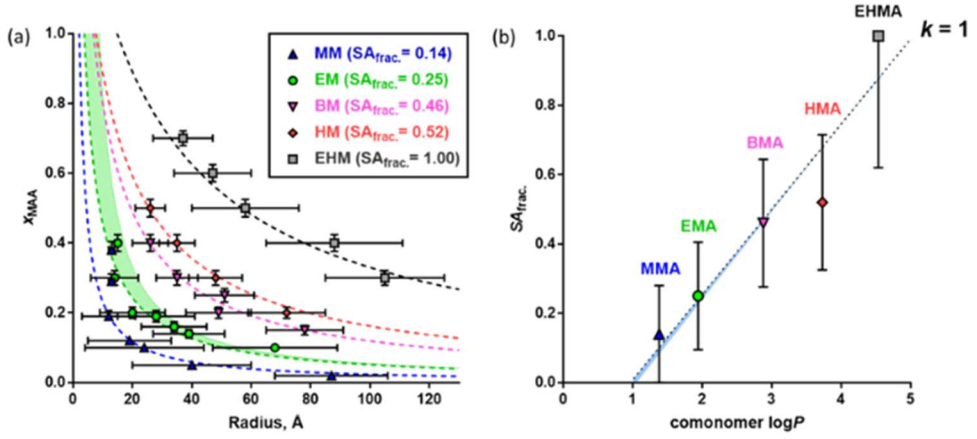

Figure 3. (a) Relationship between the mole fraction of MAA units in the amphiphilic statistical copolymer chains, x_{MAA}, and the corresponding mean radius of the nanoparticles formed by the self-assembly of such copolymers in aqueous solution: experimental data (symbols) fitted by the PSC model (dashed lines) assuming that $k = 1$ (eqs 1−3). Color-coded values of the MAA fractional surface coverage ($SA_{frac.}$) obtained by the PSC model fitting are given for each series. The green shaded area indicates the effect of nanoparticle hydration on the PSC model. The bars plotted for each point in the direction of the x-axis correspond to the standard deviation in the mean nanoparticle radius. (b) Plot of $SA_{frac.}$ values obtained by fitting the PSC model for each copolymer series (symbols) against log P for the respective alkyl methacrylate comonomers: a linear fit to the data (dotted line) was obtained using the equation $SA_{frac.} = 0.246 \times \log P - 0.237$. The narrow blue shaded area indicates the minimal effect of nanoparticle hydration on the linear relationship. The bars plotted for each point indicate the range of $SA_{frac.}$ values estimated from the standard deviation in the nanoparticle radius.

The spherical nanoparticle surface area can be calculated from the particle radius (R). Thus, if $SA_{frac.}$ is independent of the nanoparticle size, the mean number of anionic B groups per nanoparticle ($N_{B,p}$) can be estimated using

$$N_{B,p} = 1/k \times \frac{4\pi R^2 \times SA_{frac.}}{CS_B} \quad (1)$$

where CS_B is the cross-sectional area of a single B repeat unit calculated from the approximate volume of a single B unit, V_B ($CS_B = V_B^{2/3}$) and k is the fraction of the B groups located at the particle surface. k equals 1 when all of the anionic B groups are located at the nanoparticle surface. Alternatively, if all of the B units are buried within the nanoparticle cores, k equals 0. In the latter case, the nanoparticles are not colloidally stable ($N_{B,p}$ tends to infinity, suggesting that an infinitely large particle would be required to form a stable dispersion). Since the size of particles formed by statistical copolymers is independent of their molecular weight, the chosen definition of $N_{B,p}$ (eq 1) enables the molecular weight to be excluded from the calculation.

The mean number of hydrophobic alkyl methacrylate (A) repeat units can be obtained from the volume of the hydrophobic domain within a nanoparticle, which is equal to the difference between the overall nanoparticle volume and the volume occupied by the B repeat units in the same nanoparticle, divided by the approximate volume of a single hydrophobic unit (V_A)

$$N_{A,p} = \frac{4/3\pi R^3 - \left(1/k \times \frac{4\pi R^2 \times SA_{frac.} \times V_B}{CS_B}\right)}{V_A} \quad (2)$$

Using both $N_{B,p}$ and $N_{A,p}$, the mole fraction of B groups in a nanoparticle, x_B, can be calculated

$$x_B = \frac{N_{B,p}}{N_{B,p} + N_{A,p}} \quad (3)$$

This parameter is equivalent to the B mole fraction in the copolymer so eqs 1−3 provide a relationship between the particle radius and the copolymer composition. If the B content is sufficiently high, then the amphiphilic copolymer chains undergo intramolecular hydrophobic interactions to form SCNPs or self-folded chains. At this point, the particle volume is simply equal to the volume of a single copolymer chain. Hence, the corresponding copolymer compositions do not fit the PSC model (eqs 1−3) because the condition that the particle size is independent of polymer molecular weight is no longer valid. It follows that the data points corresponding to SCNPs should be excluded from any analysis based on this model. Furthermore, if the ionic comonomer content is sufficiently high, then the individual copolymer chains will be molecularly dissolved. Conversely, as the mole fraction of B tends toward zero then R tends to infinity, with infinitely large particles corresponding to the macroscopic precipitation that is observed when the mole fraction of B is insufficient to confer colloidal stability (Figure S8).

Bearing these important caveats in mind, the proposed PSC model was initially used to fit the mean particle radius for each anionic ASC series (Table 2) and hence predict the mean surface area fraction for the MAA repeat units (Figure 3a). Initially, it was assumed that all of the MAA units were located on the nanoparticle surface, i.e., $k = 1$. This simple model provided a good fit to all of the experimental data, with larger nanoparticles always being formed by copolymers with lower acid contents. Such good agreement between the experimental data and the model fit for the five series of anionic copolymers (Figure 3a) validates the assumption that a constant surface charge density is required for a particular pair of comonomers to form self-assembled nanoparticles, regardless of their molar ratio. Furthermore, the PSC model provided good data fits regardless of whether the copolymerization has pseudo-living or nonliving character (i.e., RAFT polymerization vs FRP, Figure S11). This indicates that this model is insensitive to the copolymer molecular weight distribution.

https://dx.doi.org/10.1021/acs.macromol.0c02341
Macromolecules 2021, 54, 1425−1440

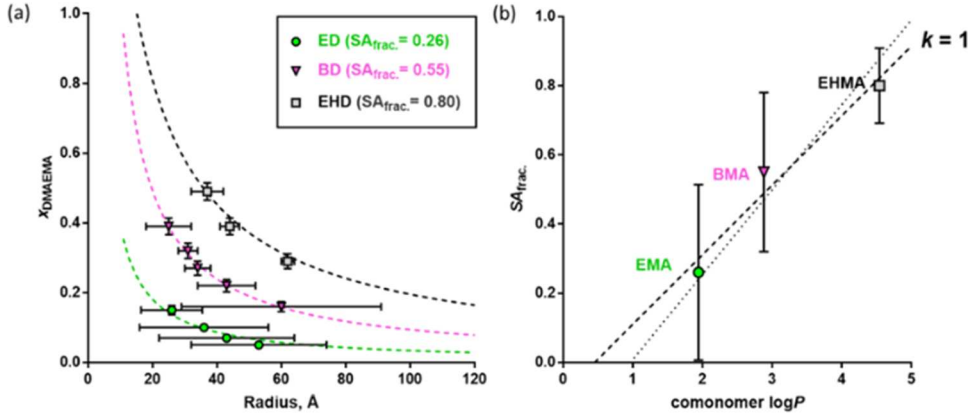

Figure 4. (a) Relationship between the mole fraction of DMAEMA repeat units in the amphiphilic statistical copolymer chains, x_{DMAEMA}, and the corresponding mean radius of nanoparticles formed by their self-assembly in an aqueous solution: experimental data (symbols) are fitted by the PSC model (dashed lines) assuming that $k = 1$ (eqs 1−3). Color-coded DMAEMA fractional surface coverages ($SA_{frac.}$) obtained by PSC model fits are given for each series. The bars plotted for each point in the direction of the x-axis correspond to the standard deviation in the nanoparticle radius. (b) Plot of $SA_{frac.}$ values obtained by fitting the PSC model for each copolymer series (symbols) against $\log P$ for the respective alkyl methacrylate comonomers: a linear fit to the data (dotted line) was obtained using the equation $SA_{frac.} = 0.201 \times \log P - 0.091$. The linear trend of the anionic series (from Figure 3b) is also shown for comparison (dotted line). The bars plotted for each point indicate the range of $SA_{frac.}$ estimated from the standard deviation in the nanoparticle radius.

The PSC model assumes that there is no solvent present within the nanoparticles. This has been confirmed for the BM series[34] and is also likely to be the case for the more hydrophobic comonomers (i.e., HMA and EHMA). However, it may not necessarily be true for less hydrophobic comonomers such as MMA and EMA. In this latter case, the effect of nanoparticle hydration on the PSC model can be explored by assuming that x_{sol} is proportional to x_B (i.e., $x_{sol} = \gamma \times x_B$). Even for an extreme scenario, where the x_{sol} is equal to x_B ($\gamma = 1$), the effect of nanoparticle hydration on this simple PSC model is minimal (Figure 3a, green shaded area), so any deviation from the modeled $SA_{frac.}$ is negligible [EM $SA_{frac.}$ = 0.25 ($\gamma = 0$) and 0.23 ($\gamma = 1$)].

For the copolymer series with differing hydrophobic A units (Figure 3a), incorporating a more hydrophobic comonomer at a given (fixed) MAA content always produces larger nanoparticles. This is because of the difference in critical surface charge density required for colloidal stability. For example, the PSC model indicates that the HM copolymer series requires 52% surface coverage of the nanoparticles by MAA units, whereas only 14% surface coverage is required for the MM copolymer series (Figure 3a). These observations are consistent with the greater hydrophobic character of HMA compared to MMA. To achieve a higher surface charge density for the same mole fraction of MAA units, the copolymer aggregation number must increase to reduce the particle surface-to-volume ratio and hence increase the number of surface-confined MAA units. This leads to a larger overall copolymer volume per nanoparticle and hence a corresponding increase in the mean nanoparticle radius (Figure 3a, compare nanoparticle radii observed for copolymers with comparable MAA contents). For the EHM series, the modeled $SA_{frac.}$ reaches the PSC model's theoretical limit of 1 (i.e., the entire nanoparticle surface is covered with MAA units), which is not physically realistic. It is rather unlikely that all of the MAA units are simultaneously co-located at the nanoparticle surface owing to the statistical distribution of this comonomer along the copolymer backbone. Hence, the earlier assumption that $k = 1$ may not be valid. If $k < 1$, then the modeled $SA_{frac.}$ will be reduced accordingly so the EHM series will no longer achieve the maximum $SA_{frac.}$ of 1. It should also be noted that the dispersions were formulated so that the MAA units were fully ionized (pH ∼ 8). However, it is probable that a reduction of MAA ionization will lead to a higher $SA_{frac.}$ being required for stabilization and could eventually lead to mass precipitation due to insufficient charge stability. Although this simple PSC model provides good fits to the experimental data, it would be more useful to relate the model parameters to the hydrophobic character of the alkyl methacrylate comonomer. The partition coefficient ($\log P$) is commonly used to rank the hydrophobic character of compounds: it is defined as the concentration distribution of a compound between two immiscible solvents, typically water and n-octanol, and can be used to quantify the hydrophobicity of methacrylic monomers.[64−67] Recently, this approach has also been used to predict suitable water-miscible monomers for RAFT aqueous dispersion polymerization formulations.[67] The relationship between $\log P$ for the hydrophobic comonomer and $SA_{frac.}$, as determined from the PSC model fitting assuming that all of the MAA units are located at the nanoparticle surface ($k = 1$) (Figure 3a), can be satisfactorily fitted using a linear function: [$SA_{frac.} = 0.246 \times \log P - 0.237$; $R^2 = 0.91$] (Figure 3b). This equation can be used to predict the self-assembly behavior of other methacrylic ASCs: given the $\log P$ of the hydrophobic comonomer, a corresponding $SA_{frac.}$ may be estimated and then the nanoparticle size is determined using the PSC model (eqs 1−3).

The PSC model was also used to establish the size-composition relationship for the cationic copolymer series (Table 3). Good data fits are obtained (Figure 4a), justifying the hypothesis that the nanoparticle size is determined by achieving the critical surface charge density required for a stable colloidal dispersion. Furthermore, the critical surface charge density or fraction of the nanoparticle surface area covered by DMAEMA repeat units ($SA_{frac.}$) can be determined using the PSC model. In agreement with the anionic copolymer series, $SA_{frac.}$ increases when using more hydrophobic alkyl methacrylate comonomers. If $k = 1$, only 26% of the nanoparticle surface needs to be covered by DMAEMA repeat units to form stable colloidal dispersions for the ED

https://dx.doi.org/10.1021/acs.macromol.0c02341
Macromolecules 2021, 54, 1425−1440

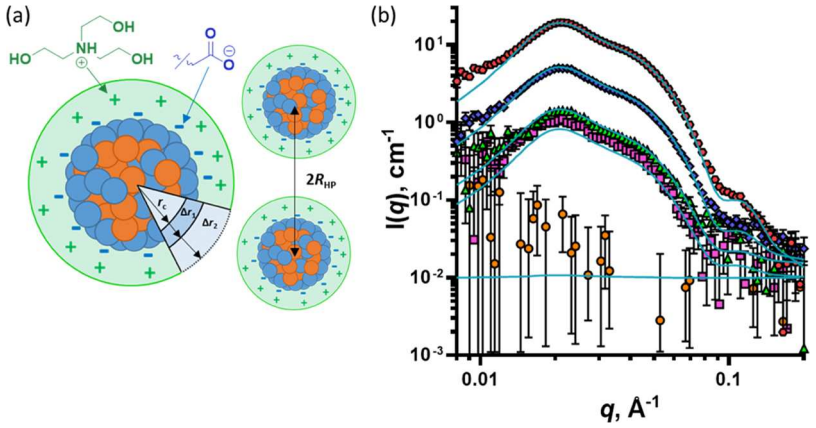

Figure 5. (a) Schematic cartoon describing the core−shell−shell model used to fit the SANS data that accounts for the preferential location of the BMA units within the core, the preferential location of the MAA units at the particle surface (inner shell), and the hydrated outer shell of TEA cations surrounding the nanoparticles, where r_c is the nanoparticle core radius, Δr_1 is the thickness of the MAA-rich inner shell, Δr_2 is the thickness of the cation outer shell, and $2R_{HP}$ is the mean interparticle distance. (b) SANS patterns recorded for 2.0% w/w aqueous dispersions of BM_{8020} in five different H_2O/D_2O binary mixtures (symbols). For this contrast variation experiment, the solvent SLD corresponds to -0.56×10^{10} cm^{-2} (H_2O; pink squares), 0.58×10^{10} cm^{-2} (83.5:16.5 H_2O/D_2O; orange circles), 2.20×10^{10} cm^{-2} (60:40 H_2O/D_2O; green triangles), 3.58×10^{10} cm^{-2} (40:60 H_2O/D_2O; blue diamonds), and 6.33×10^{10} cm^{-2} (D_2O; red hexagons). All five data sets were fitted simultaneously using a spherical core−shell−shell nanoparticle model (eqs S17−S29) (turquoise solid lines).

series. On the other hand, 80% coverage is required for the EHD series (Figure 4a) since EHMA is a much more hydrophobic comonomer than EMA.

The log P values for the hydrophobic comonomers were plotted against SA_{frac}, as determined from the PSC model by assuming $k = 1$. In analogy with the anionic copolymer series, a linear function could be fitted to the data [$SA_{frac.} = 0.201 \times \log P - 0.091$; $R^2 = 0.96$] (Figure 4b). This relationship between log P and $SA_{frac.}$ can be used to predict the behavior of other P(*A-stat*-DMAEMA) amphiphilic copolymers. Furthermore, a strong correlation between the linear fits is observed for the anionic and cationic copolymer series (Figure 4b, dashed line vs solid line). Thus, the PSC model appears to be universal for describing the aqueous self-assembly behavior of charged amphiphilic statistical copolymers that comprise a pair of hydrophilic and hydrophobic comonomers.

Determination of Internal Particle Structure Using Contrast Variation SANS. Since the ionic comonomer repeat units are statistically distributed along each copolymer chain, the formation of well-defined hydrophilic and hydrophobic domains within the nanoparticles seems unlikely. Indeed, satisfactory fits to the scattering patterns recorded for these amphiphilic copolymer nanoparticles can be obtained when they are described as homogeneous spheres (Figures 1, 2, S6, and S10). However, according to the PSC model analysis (Figures 3 and 4), the MAA (or DMAEMA) repeat units should be located preferentially at the nanoparticle surface to confer sufficient surface charge density for colloidal stability. Therefore, it is likely that such nanoparticles actually comprise a thin "shell-like" surface layer enriched with the ionic comonomer and a "core-like" region composed mainly of the hydrophobic alkyl methacrylate comonomer (Figure 5a). In the initial analysis (Figures 3a and 4a), it was assumed that all of the ionic comonomer repeat units were located at the nanoparticle surface ($k = 1$). However, their statistical distribution along the copolymer chains suggests that at least some of these ionic groups may be located within the interior of the nanoparticles (i.e., $k < 1$). In this respect, experimental determination of the mole fraction of the ionic comonomer repeat units at the nanoparticle surface would enable the refinement of the PSC model.

Accordingly, contrast variation SANS experiments were performed on nanoparticles formed by one of the anionic copolymers (BM_{8020}) to examine their internal structure. This particular copolymer was chosen for SANS measurements because it is representative: BMA exhibits an intermediate log P value and BM_{8020} lies in the middle of the BMA copolymer series. In addition, it was previously demonstrated that the solvent (water) does not penetrate the BM nanoparticles,[34] which should simplify the SANS analysis. Since H_2O and D_2O exhibit differing neutron SLDs (-0.56×10^{10} and 6.33×10^{10} cm^{-2}, respectively),[68−75] H_2O/D_2O mixtures can be used to adjust the SLD of the solvent environment (ξ_{sol}) to highlight any hydrophilic or hydrophobic domains that may be present in the copolymer nanoparticles. Thus, 2% w/w dispersions of BM_{8020} were prepared in H_2O, D_2O, and several H_2O/D_2O mixtures (comprising 83.5:16.5, 60:40, and 40:60 compositions by volume, which correspond to ξ_{sol} values of 0.58×10^{10}, 2.20×10^{10}, and 3.58×10^{10} cm^{-2}, respectively, see eq S23). TEA was added during the formulation of the dispersions so that all MAA units were ionized (pH 8). SANS patterns were recorded for all five dispersions (Figure 5b). Following the general approach and principles adopted for the SAXS data analysis (Figure 1), each SANS pattern could be fitted reasonably well using a core−shell model.

Assuming that the MAA comonomer is preferentially located near the nanoparticle surface, a more sophisticated spherical core−shell−shell model (Figure 5a) should be more appropriate for analyzing the SANS patterns. Thus, all patterns were fitted using the core−shell−shell model (eqs S17−S29) where the core corresponds to a BMA-rich region, the inner shell is the MAA-rich anionic surface layer, and the outer shell represents the protonated TEA counterions (Figure 5). To account for interactions between such anionic nanoparticles, the Hayter−Penfold approximation for a charged sphere structure factor (eq S33) was included in the intensity equation (eq S34). To ensure that the model was physically

https://dx.doi.org/10.1021/acs.macromol.0c02341
Macromolecules 2021, 54, 1425−1440

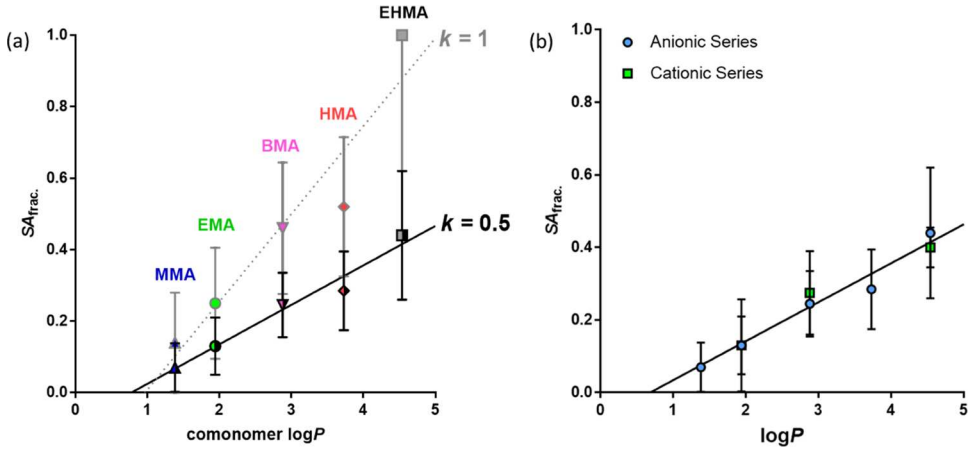

Figure 6. (a) Linear relationship between the log P values for the hydrophobic alkyl methacrylate comonomers and the $SA_{frac.}$ evaluated by PSC model fitting. The open symbols correspond to the previously assumed scenario[34] (Figure 3b) in which the MAA units are exclusively located at the nanoparticle surface (k = 1), while the half closed symbols correspond to the more physically realistic scenario indicated by contrast variation SANS experiments (k = 0.5). These two data sets were fitted using $SA_{frac.} = 0.246 \times \log P - 0.237$ (dotted line) and $SA_{frac.} = 0.110 \times \log P - 0.085$ (solid line) linear functions, respectively. (b) Linear relationship between the log P values for the various hydrophobic alkyl methacrylate comonomers and the $SA_{frac.}$ evaluated by PSC model fitting, where k = 0.5. The blue circle symbols correspond to the anionic (MAA) copolymer series, and the green square symbols correspond to the cationic (DMAEMA) copolymer series. The black line shows the linear relationship obtained when combining these two series [$SA_{frac.} = 0.107 \times \log P - 0.073$, $R^2 = 0.96$]. The bars plotted for each point indicate the range of $SA_{frac.}$ values estimated using the standard deviation for the nanoparticle radius.

realistic, a number of constraints were incorporated. The 80:20 BMA/MAA copolymer composition was fixed, and the overall nanoparticle composition should be identical to that of the copolymer. Thus, the SLDs of the core and the first shell, which are each formed by redistribution of the comonomer repeat units within the nanoparticles, were related to each other via the copolymer composition (eqs S24−S29). In other words, if the nanoparticle shell is MAA-rich, then the particle core must be depleted in MAA to the same extent. Furthermore, the inner shell thickness (Δr_1) was fixed at 5 Å, which corresponds to the approximate dimensions of a single MAA repeat unit (eq S30). Finally, like the SAXS analysis, the outer shell thickness was fixed at 6 Å, which corresponds to the approximate dimensions of an individual protonated TEA counterion, and the SLD of this cationic shell was calculated from the fraction of MAA repeat units located at the nanoparticle surface.

It is worth noting that analysis of the SANS and SAXS patterns recorded for the BM_{8020} dispersion using a simple sphere model (eq S7) yielded apparently inconsistent nanoparticle dimensions. More specifically, SAXS indicated a mean radius of 58 Å while SANS suggested a mean radius of 49 Å. This difference is attributed to the presence of the TEA cation shell as its SLD contrast in respect to the surrounding solvent is significantly higher for X-rays than for neutrons. This observation highlights the presence of the cationic TEA shell surrounding the anionic nanoparticles. Using a core−shell model to fit the SAXS pattern of BM_{8020} dispersions, a nanoparticle mean radius of 49 Å was calculated (Table 2). This is in good agreement with the mean radius reported by SANS, which is less sensitive to the cationic TEA shell. Initial analysis of the contrast variation SANS data performed for the five patterns individually indicated that the SLD of the first shell was always higher than that of the core. This suggests that the MAA residues (which have a higher neutron SLD than the BMA residues) are preferentially located at (or near) the surface. However, the first shell SLDs obtained for each of the measurements were spread over a relatively broad range of values. Thus, all contrast variation SANS patterns were fitted simultaneously to provide more statistically robust and reliable information. To achieve this, it was assumed that all copolymer dispersions differ only in terms of their SLD contrast relative to the aqueous continuous phase. Thus, SANS patterns were fitted simultaneously using certain global parameters for the contrast series such as mean nanoparticle radius (and its associated standard deviation), inner shell thickness, outer shell thickness, degree of hydration of the outer shell (calculated based on the proportion of surface MAA units as for the SAXS analysis), and the mean SLD for the nanoparticle core and shell components. A plugin describing the structural model (eqs S17−S29) has been coded for the SASfit package[76] to perform this analysis. Satisfactory fits were obtained for all five SANS scattering patterns (Figure 5b), allowing the mean radius for the nanoparticle core and SLDs for the nanoparticle core and shell to be determined (R_c = 41 Å, $\xi_{core} = 0.61 \times 10^{10}$ cm^{-2}, and $\xi_{shell} = 0.72 \times 10^{10}$ cm^{-2}, respectively).

According to this SANS analysis, the nanoparticle core has a lower neutron SLD than the shell ($\xi_{core} < \xi_{shell}$). By comparing these values with those obtained for ξ_{BMA} and ξ_{MAA} (0.55×10^{10} and 1.38×10^{10} cm^{-2}, respectively), calculated using respective mass densities of PBMA and PMAA (ρ_{BMA} = 1.05 g cm^{-3} and ρ_{MAA} = 1.25 g cm^{-3}), it can be concluded that approximately half of the MAA residues are located within the nanoparticle cores while the remainder are within the thin shell at the nanoparticle surface (eqs S36−S38). Thus, the copolymer nanoparticle surface is certainly enriched with anionic MAA residues, but only about 50% of the available MAA groups are actually located there (i.e., $k \sim 0.5$). This is physically reasonable as the statistically distributed MAA residues are constrained within the copolymer chains; this reduces their mobility and results in a significant proportion remaining within the nanoparticle cores.

These SANS results enable (i) the core−shell model used for analyzing the SAXS data to be adjusted and (ii) the PSC model (eqs 1−3, Figure 3) to be calibrated with a realistic estimate of the proportion of ionic comonomer residues

https://dx.doi.org/10.1021/acs.macromol.0c02341
Macromolecules 2021, 54, 1425−1440

actually located at the nanoparticle surface. Accordingly, the numerical value of k used in the core−shell model was reduced from 1 to 0.5 to calculate a more realistic SLD for the cation shell. The entire anionic series was appropriately remodeled for k = 0.5, and new particle sizes were calculated (Table S3). Similarly, the PSC model (eqs 1−3) was adjusted using k = 0.5. This dual approach produced new $SA_{frac.}$ values based on the real composition of the particle surfaces measured by SANS. Moreover, the linear relationship between log P and $SA_{frac.}$ remained valid for the new data (Figure 6a). A new linear regression was fit to the data, yielding $SA_{frac.} = 0.110 \times \log P - 0.085$. This new equation can be used to predict particle size if it is assumed that k remains constant in the PSC model.

The cationic copolymer series was similarly reanalyzed. Combining the data obtained for the anionic and cationic series (Figure 6b) produces a linear relationship (R^2 = 0.96) between log P and the modeled $SA_{frac.}$ (k = 0.5). This highlights the self-consistency of the refined PSC model. Finally, the linear equation representing the relationship between log P for the hydrophobic comonomer and the modeled $SA_{frac.}$ for the MAA copolymers crosses the x-axis (i.e., $SA_{frac.} = 0$) at a log P value of between 0.5 and 1. This suggests that, at this log P value, the nanoparticles would require no ionic comonomer to be located at the surface to confer colloidal stability. Alternatively, a comonomer exhibiting a log P of between 0.5 and 1, or below 0.5, would not be sufficiently hydrophobic to induce self-assembly, hence, such copolymers would remain molecularly dissolved in an aqueous solution.

CONCLUSIONS

A series of five alkyl methacrylates were statistically copolymerized in turn with either anionic MAA or cationic DMAEMA via RAFT polymerization to generate a library of amphiphilic statistical copolymers with varying MAA (or DMAEMA) content and tunable hydrophobic character. Additionally, a series of P(BMA-*stat*-MAA) copolymers were prepared using conventional free-radical polymerization to examine the effect of a relatively broad molecular weight distribution on statistical copolymer self-assembly. Kinetic studies confirmed that the hydrophobic and hydrophilic comonomers react at similar rates when copolymerizations were performed in concentrated solution in either IPA or dioxane. This indicates that an approximately statistical distribution of hydrophilic comonomer within the copolymer chains can be achieved using a one-shot batch synthesis protocol.

A solvent-switch technique was used to obtain aqueous dispersions of self-assembled copolymer nanoparticles, whereby each copolymer was first molecularly dissolved in IPA and then slowly diluted using either an alkaline or acidic aqueous solution depending on the type of hydrophilic comonomer. SAXS analysis confirmed that alkyl methacrylate-rich statistical copolymers formed larger nanoparticles, regardless of the nature of the hydrophilic comonomer. On the other hand, if the copolymer chains have a sufficiently high hydrophilic comonomer content, distinctly anisotropic single-chain nanoparticles can be obtained via intramolecular hydrophobic interactions. When targeting a fixed copolymer composition, using a more hydrophobic comonomer produced larger spherical nanoparticles. Contrast variation SANS studies performed on P(BMA-*stat*-MAA) copolymer nanoparticles enabled their internal structure to be determined. Such nanoparticles possess a core−shell-like morphology in which anionic MAA residues are preferentially located within the shell, thus conferring colloidal stability. However, owing to their statistical distribution along the copolymer chains, only about 50% of the available MAA residues can access the nanoparticle surface, with the remaining anionic residues being trapped within the nanoparticle cores.

The previously proposed particle surface charge model[34] was applied to the wide range of statistical copolymer dispersions prepared in this study. This revealed a strong correlation between the chemical structure of the hydrophobic comonomer and the surface charge density required to stabilize the copolymer nanoparticles. This model is remarkably consistent with the experimental SAXS data obtained for each copolymer, regardless of the type of hydrophilic comonomer or the molecular weight distribution. Importantly, it enables the nanoparticle size to be reliably predicted for a given copolymer composition. SANS studies indicate that approximately 50% of the hydrophilic comonomer repeat units is preferentially located at the nanoparticle surface. There is a linear relationship between $SA_{frac.}$ (the fraction of the nanoparticle surface covered by the hydrophile component) calculated using the PSC model and the log P value for the hydrophobic comonomer. Moreover, this PSC model is valid for both cationic and anionic amphiphilic statistical copolymers and is remarkably insensitive to the breadth of the copolymer molecular weight distribution. The PSC model offers a clear set of design rules for controlling statistical copolymer particle size, which can be adjusted via the copolymer composition in a highly convenient one-shot one-pot synthesis. This is significantly simpler than the control of diblock copolymer particle size based on copolymer composition and molecular weight and also requiring a multistage synthesis of the molecules. In summary, this study provides important new insights regarding the aqueous self-assembly of amphiphilic statistical copolymers: the reproducible and predictable control over nanoparticle size that is observed even for relatively ill-defined chains means that such copolymers should be considered as an attractive alternative to diblock copolymers for a range of industrial applications.

ASSOCIATED CONTENT

Supporting Information

The Supporting Information is available free of charge at https://pubs.acs.org/doi/10.1021/acs.macromol.0c02341.

Kinetic data for the polymerizations, TEM images, further SAXS analysis, and SAXS models (PDF)

AUTHOR INFORMATION

Corresponding Authors

Sebastian G. Spain − *Department of Chemistry, The University of Sheffield, Sheffield S3 7HF, U.K.*; orcid.org/0000-0001-7241-5713; Email: s.g.spain@sheffield.ac.uk

Oleksandr O. Mykhaylyk − *Department of Chemistry, The University of Sheffield, Sheffield S3 7HF, U.K.*; orcid.org/0000-0003-4110-8328; Email: o.mykhaylyk@sheffield.ac.uk

Authors

Thomas J. Neal − *Department of Chemistry, The University of Sheffield, Sheffield S3 7HF, U.K.*

https://dx.doi.org/10.1021/acs.macromol.0c02341
Macromolecules 2021, 54, 1425−1440

Andrew J. Parnell − *Department of Physics and Astronomy, The University of Sheffield, Sheffield S3 7RH, U.K.;* orcid.org/0000-0001-8606-8644
Stephen M. King − *ISIS Pulsed Neutron and Muon Source, STFC Rutherford Appleton Laboratory, Didcot, Oxon OX11 0QX, U.K.;* orcid.org/0000-0003-3386-9151
Deborah L. Beattie − *Department of Chemistry, The University of Sheffield, Sheffield S3 7HF, U.K.*
Martin W. Murray − *AkzoNobel Decorative Paints, Slough, Berkshire SL2 5DS, U.K.*
Neal S. J. Williams − *AkzoNobel Decorative Paints, Slough, Berkshire SL2 5DS, U.K.*
Simon N. Emmett − *AkzoNobel Decorative Paints, Slough, Berkshire SL2 5DS, U.K.*
Steven P. Armes − *Department of Chemistry, The University of Sheffield, Sheffield S3 7HF, U.K.;* orcid.org/0000-0002-8289-6351

Complete contact information is available at: https://pubs.acs.org/10.1021/acs.macromol.0c02341

Author Contributions

The manuscript was written through the contributions of all authors. All authors have given approval to the final version of the manuscript.

Notes

The authors declare no competing financial interest.

■ ACKNOWLEDGMENTS

AkzoNobel (Slough, U.K.) and EPSRC (EP/L016281/1) are thanked for funding a CDT Ph.D. CASE studentship for T.J.N. O.O.M. and S.P.A. thank EPSRC for the capital equipment grant to purchase the laboratory-based Xenocs/Excillum SAXS beamline used for characterizing the studied copolymer dispersions (EP/M028437/1). Dr. M. J. Derry is thanked for his help in calculating the nano-object surface area fraction covered by MAA.

■ ABBREVIATIONS

SAXS, small-angle X-ray scattering; SANS, small-angle neutron scattering; PSC, particle surface charge (model); ASC, amphiphilic statistical copolymers

■ REFERENCES

(1) Duan, H.; Donovan, M.; Foucher, A.; Schultze, X.; Lecommandoux, S. Multivalent and Multifunctional Polysaccharide-Based Particles for Controlled Receptor Recognition. *Sci. Rep.* **2018**, *8*, No. 14730.
(2) Kai, D.; Chua, Y. K.; Jiang, L.; Owh, C.; Chan, S. Y.; Loh, X. J. Dual Functional Anti-Oxidant and SPF Enhancing Lignin-Based Copolymers as Additives for Personal and Healthcare Products. *RSC Adv.* **2016**, *6*, 86420−86427.
(3) Hartmann, S.; Nuhn, L.; Palitzsch, B.; Glaffig, M.; Stergiou, N.; Gerlitzki, B.; Schmitt, E.; Kunz, H.; Zentel, R. CpG-Loaded Multifunctional Cationic Nanohydrogel Particles as Self-Adjuvanting Glycopeptide Antitumor Vaccines. *Adv. Healthcare Mater.* **2015**, *4*, 522−527.
(4) Geng, Y.; Discher, D. E.; Justynska, J.; Schlaad, H. Grafting Short Peptides onto Polybutadiene-Block-Poly(Ethylene Oxide): A Platform for Self-Assembling Hybrid Amphiphiles. *Angew. Chem., Int. Ed.* **2006**, *45*, 7578−7581.
(5) Kim, Y.; Dalhaimer, P.; Christian, D. A.; Discher, D. E. Polymeric Worm Micelles as Nano-Carriers for Drug Delivery. *Nanotechnology* **2005**, *16*, S484−S491.
(6) Ahmed, F.; Discher, D. E. Self-Porating Polymersomes of PEG-PLA and PEG-PCL: Hydrolysis-Triggered Controlled Release Vesicles. *J. Controlled Release* **2004**, *96*, 37−53.
(7) Christian, D. A.; Tian, A.; Ellenbroek, W. G.; Levental, I.; Rajagopal, K.; Janmey, P. A.; Liu, A. J.; Baumgart, T.; Discher, D. E. Spotted Vesicles, Striped Micelles and Janus Assemblies Induced by Ligand Binding. *Nat. Mater.* **2009**, *8*, 843−849.
(8) Peng, L.; Fang, Z.; Li, J.; Wang, L.; Bruck, A. M.; Zhu, Y.; Zhang, Y.; Takeuchi, K. J.; Marschilok, A. C.; Stach, E. A.; et al. Two-Dimensional Holey Nanoarchitectures Created by Confined Self-Assembly of Nanoparticles via Block Copolymers: From Synthesis to Energy Storage Property. *ACS Nano* **2018**, *12*, 820−828.
(9) Lin, Z.; Tian, H.; Xu, F.; Yang, X.; Mai, Y.; Feng, X. Facile Synthesis of Bowl-Shaped Nitrogen-Doped Carbon Hollow Particles Templated by Block Copolymer "Kippah Vesicles" for High Performance Supercapacitors. *Polym. Chem.* **2016**, *7*, 2092−2098.
(10) Costa, J. R. C.; Correia, C.; Góis, J. R.; Silva, S. M. C.; Antunes, F. E.; Moniz, J.; Serra, A. C.; Coelho, J. F. J. Efficient Dispersion of TiO2 Using Tailor Made Poly(Acrylic Acid) − Based Block Copolymers, and Its Incorporation in Water Based Paint Formulation. *Prog. Org. Coat.* **2017**, *104*, 34−42.
(11) Martín-Fabiani, I.; Fortini, A.; Lesage De La Haye, J.; Koh, M. L.; Taylor, S. E.; Bourgeat-Lami, E.; Lansalot, M.; D'Agosto, F.; Sear, R. P.; Keddie, J. L. PH-Switchable Stratification of Colloidal Coatings: Surfaces "on Demand. *ACS Appl. Mater. Interfaces* **2016**, *8*, 34755−34761.
(12) Mates, J. E.; Ibrahim, R.; Vera, A.; Guggenheim, S.; Qin, J.; Calewarts, D.; Waldroup, D. E.; Megaridis, C. M. Environmentally-Safe and Transparent Superhydrophobic Coatings. *Green Chem.* **2016**, *18*, 2185−2192.
(13) Mai, Y.; Eisenberg, A. Self-Assembly of Block Copolymers. *Chem. Soc. Rev.* **2012**, *41*, 5969−5985.
(14) Blanazs, A.; Armes, S. P.; Ryan, A. J. Self-Assembled Block Copolymer Aggregates: From Micelles to Vesicles and Their Biological Applications. *Macromol. Rapid Commun.* **2009**, *30*, 267−277.
(15) Gröschel, A. H.; Walther, A. Block Copolymer Micelles with Inverted Morphologies. *Angew. Chem., Int. Ed.* **2017**, *56*, 10992−10994.
(16) Zhang, Y.; Wang, Z.; Matyjaszewski, K.; Pietrasik, J. Evolution of Morphology of POEGMA-b-PBzMA Nano-Objects Formed by PISA. *Macromol. Rapid Commun.* **2019**, *40*, No. 1800331.
(17) Rieger, J. Guidelines for the Synthesis of Block Copolymer Particles of Various Morphologies by RAFT Dispersion Polymerization. *Macromol. Rapid Commun.* **2015**, *36*, 1458−1471.
(18) Wang, E.; Lu, J.; Bates, F. S.; Lodge, T. P. Effect of Corona Block Length on the Structure and Chain Exchange Kinetics of Block Copolymer Micelles. *Macromolecules* **2018**, *51*, 3563−3571.
(19) Nesvadba, P. Radical Polymerization in Industry. In *Encyclopedia of Radicals in Chemistry, Biology and Materials*; John Wiley & Sons: New Jersey, 2012.
(20) Wu, X.; Qiao, Y.; Yang, H.; Wang, J. Self-Assembly of a Series of Random Copolymers Bearing Amphiphilic Side Chains. *J. Colloid Interface Sci.* **2010**, *349*, 560−564.
(21) Kawata, T.; Hashidzume, A.; Sato, T. Micellar Structure of Amphiphilic Statistical Copolymers Bearing Dodecyl Hydrophobes in Aqueous Media. *Macromolecules* **2007**, *40*, 1174−1180.
(22) Zhu, X.; Liu, M. Self-Assembly and Morphology Control of New l -Glutamic Acid-Based Amphiphilic Random Copolymers: Giant Vesicles, Vesicles, Spheres, and Honeycomb Film. *Langmuir* **2011**, *27*, 12844−12850.
(23) Tian, F.; Yu, Y.; Wang, C.; Yang, S. Consecutive Morphological Transitions in Nanoaggregates Assembled from Amphiphilic Random Copolymer via Water Driven Micellization and Light-Triggered Dissociation. *Macromolecules* **2008**, *41*, 3385−3388.
(24) Sun, G.; Zhang, M.; He, J.; Ni, P. Synthesis of Amphiphilic Cationic Copolymers Poly[2-(Methacryloyloxy)Ethyl Trimethylammonium Chloride-Co-Stearyl Methacrylate] and Their Self-Assembly

Behavior in Water and Water-Ethanol Mixtures. *J. Polym. Sci., Part A: Polym. Chem.* **2009**, *47*, 4670−4684.
(25) Stephan, T.; Muth, S.; Schmidt, M. Shape Changes of Statistical Copolymacromonomers: From Wormlike Cylinders to Horseshoe- and Meanderlike Structures. *Macromolecules* **2002**, *35*, 9857−9860.
(26) Ilhan, F.; Galow, T. H.; Gray, M.; Clavier, G.; Rotello, V. M. Giant Vesicle Formation through Self-Assembly of Complementary Random Copolymers [10]. *J. Am. Chem. Soc.* **2000**, *122*, 5895−5896.
(27) Liu, X.; Kim, J.-S.; Wu, J.; Eisenberg, A. Bowl-Shaped Aggregates from the Self-Assembly of an Amphiphilic Random Copolymer of Poly(Styrene- Co -Methacrylic Acid). *Macromolecules* **2005**, *38*, 6749−6751.
(28) Wang, J.; Zhu, J. Recent Advances in Spherical Photonic Crystals: Generation and Applications in Optics. *Eur. Polym. J.* **2013**, *49*, 3420−3433.
(29) Hattori, G.; Takenaka, M.; Sawamoto, M.; Terashima, T. Nanostructured Materials via the Pendant Self-Assembly of Amphiphilic Crystalline Random Copolymers. *J. Am. Chem. Soc.* **2018**, *140*, 8376−8379.
(30) Matsumoto, M.; Sawamoto, M.; Terashima, T. Orthogonal Folding of Amphiphilic/Fluorous Random Block Copolymers for Double and Multicompartment Micelles in Water. *ACS Macro Lett.* **2019**, *8*, 320−325.
(31) Matsumoto, M.; Terashima, T.; Matsumoto, K.; Takenaka, M.; Sawamoto, M. Compartmentalization Technologies via Self-Assembly and Cross-Linking of Amphiphilic Random Block Copolymers in Water. *J. Am. Chem. Soc.* **2017**, *139*, 7164−7167.
(32) Imai, S.; Hirai, Y.; Nagao, C.; Sawamoto, M.; Terashima, T. Programmed Self-Assembly Systems of Amphiphilic Random Copolymers into Size-Controlled and Thermoresponsive Micelles in Water. *Macromolecules* **2018**, *51*, 398−409.
(33) Hashidzume, A.; Kawaguchi, A.; Tagawa, A.; Hyoda, K.; Sato, T. Synthesis and Structural Analysis of Self-Associating Amphiphilic Statistical Copolymers in Aqueous Media. *Macromolecules* **2006**, *39*, 1135−1143.
(34) Neal, T. J.; Beattie, D. L.; Byard, S. J.; Smith, G. N.; Murray, M. W.; Williams, N. S. J.; Emmett, S. N.; Armes, S. P.; Spain, S. G.; Mykhaylyk, O. O. Self-Assembly of Amphiphilic Statistical Copolymers and Their Aqueous Rheological Properties. *Macromolecules* **2018**, *51*, 1474−1487.
(35) Semsarilar, M.; Ladmiral, V.; Blanazs, A.; Armes, S. P. Anionic Polyelectrolyte-Stabilized Nanoparticles via RAFT Aqueous Dispersion Polymerization. *Langmuir* **2012**, *28*, 914−922.
(36) Cockram, A. A.; Neal, T. J.; Derry, M. J.; Mykhaylyk, O. O.; Williams, N. S. J.; Murray, M. W.; Emmett, S. N.; Armes, S. P. Effect of Monomer Solubility on the Evolution of Copolymer Morphology during Polymerization-Induced Self-Assembly in Aqueous Solution. *Macromolecules* **2017**, *50*, 796−802.
(37) Ilavsky, J. Nika: Software for Two-Dimensional Data Reduction. *J. Appl. Crystallogr.* **2012**, *45*, 324−328.
(38) Ilavsky, J.; Jemian, P. R. Irena: Tool Suite for Modeling and Analysis of Small-Angle Scattering. *J. Appl. Crystallogr.* **2009**, *42*, 347−353.
(39) Heenan, R. K.; Penfold, J.; King, S. M. SANS at Pulsed Neutron Sources: Present and Future Prospects. *J. Appl. Crystallogr.* **1997**, *30*, 1140−1147.
(40) Arnold, O.; Bilheux, J. C.; Borreguero, J. M.; Buts, A.; Campbell, S. I.; Chapon, L.; Doucet, M.; Draper, N.; Ferraz Leal, R.; Gigg, M. A.; et al. Mantid—Data Analysis and Visualization Package for Neutron Scattering and μ SR Experiments. *Nucl. Instrum. Methods Phys. Res., Sect. A* **2014**, *764*, 156−166.
(41) Wignall, G. D.; Bates, F. S. Absolute Calibration of Small-Angle Neutron Scattering Data of a Double-Crystal Diffractometer. *J. Appl. Crystallogr.* **1987**, *20*, 28−40.
(42) Sangster, J. *Octanol-Water Partition Coefficients: Fundamentals and Physical Chemistry*, 2nd ed.; John Wiley & Sons: Chichester, 1997.
(43) Kostanski, L. K.; Keller, D. M.; Hamielec, A. E. Size-Exclusion Chromatography—A Review of Calibration Methodologies. *J. Biochem. Biophys. Methods* **2004**, *58*, 159−186.
(44) Huang, J.; Wu, X. Y. Effects of PH, Salt, Surfactant and Composition on Phase Transition of Poly(NIPAm/MAA) Nanoparticles. *J. Polym. Sci., Part A: Polym. Chem.* **1999**, *37*, 2667−2676.
(45) Gao, C.; Liu, M.; Chen, J.; Chen, C. PH- and Temperature-Responsive P(DMAEMA-GMA)-Alginate Semi-IPN Hydrogels Formed by Radical and Ring-Opening Polymerization for Aminophylline Release. *J. Biomater. Sci., Polym. Ed.* **2012**, *23*, 1039−1054.
(46) Pegg, J. C.; Czajka, A.; Hill, C.; James, C.; Peach, J.; Rogers, S. E.; Eastoe, J. Alternative Route to Nanoscale Aggregates with a PH-Responsive Random Copolymer. *Langmuir* **2017**, *33*, 2628−2638.
(47) Rawiso, M.; Zilliox, J.-G.; Demé, B.; Boué, F.; Combet, J.; Heinrich, M. SANS from Salt-Free Aqueous Solutions of Hydrophilic and Highly Charged Star-Branched Polyelectrolytes. *Polymers* **2016**, *8*, 228.
(48) Hayter, J. B.; Penfold, J. An Analytic Structure Factor for Macroion Solutions. *Mol. Phys.* **1981**, *42*, 109−118.
(49) Pedersen, J. S.; Gerstenberg, M. C. Scattering Form Factor of Block Copolymer Micelles. *Macromolecules* **1996**, *29*, 1363−1365.
(50) Percus, J. K.; Yevick, G. J. Analysis of Classical Statistical Mechanics by Means of Collective Coordinates. *Phys. Rev.* **1958**, *110*, 1−13.
(51) Moffitt, M.; Eisenberg, A. Scaling Relations and Size Control of Block Ionomer Microreactors Containing Different Metal Ions. *Macromolecules* **1997**, *30*, 4363−4373.
(52) Zhang, L.; Eisenberg, A. Multiple Morphologies and Characteristics of "crew-Cut" Micelle-like Aggregates of Polystyrene-b-Poly(Acrylic Acid) Diblock Copolymers in Aqueous Solutions. *J. Am. Chem. Soc.* **1996**, *118*, 3168−3181.
(53) Förster, S.; Zisenis, M.; Wenz, E.; Antonietti, M. Micellization of Strongly Segregated Block Copolymers. *J. Chem. Phys.* **1996**, *104*, 9956−9970.
(54) Ouchi, M.; Badi, N.; Lutz, J.-F.; Sawamoto, M. Single-Chain Technology Using Discrete Synthetic Macromolecules. *Nat. Chem.* **2011**, *3*, 917−924.
(55) Altintas, O.; Barner-Kowollik, C. Single-Chain Folding of Synthetic Polymers: A Critical Update. *Macromol. Rapid Commun.* **2016**, *37*, 29−46.
(56) Hanlon, A. M.; Lyon, C. K.; Berda, E. B. What Is Next in Single-Chain Nanoparticles? *Macromolecules* **2016**, *49*, 2−14.
(57) Lyon, C. K.; Prasher, A.; Hanlon, A. M.; Tuten, B. T.; Tooley, C. A.; Frank, P. G.; Berda, E. B. A Brief User's Guide to Single-Chain Nanoparticles. *Polym. Chem.* **2015**, *6*, 181−197.
(58) Artar, M.; Huerta, E.; Meijer, E. W.; Palmans, A. R. A. Dynamic Single Chain Polymeric Nanoparticles: From Structure to Function. In *Sequence-Controlled Polymers: Synthesis, Self-Assembly, and Properties*; Lutz, J.-F.; Meyer, T. Y.; Ouchi, M.; Sawamoto, M., Eds.; ACS Symposium Series; American Chemical Society: Washington, DC, 2014; pp 313−325.
(59) Ruiz-Pérez, L.; Pryke, A.; Sommer, M.; Battaglia, G.; Soutar, I.; Swanson, L.; Geoghegan, M. Conformation of Poiy(Methacrylic Acid) Chains in Dilute Aqueous Solution. *Macromolecules* **2008**, *41*, 2203−2211.
(60) Muroga, Y.; Yoshida, T.; Kawaguchi, S. Conformation of Poly(Methacrylic Acid) in Acidic Aqueous Solution Studied by Small Angle X-Ray Scattering. *Biophys. Chem.* **1999**, *81*, 45−57.
(61) Heitz, C.; Rawiso, M.; François, J. X-Ray Scattering Study of a Poly(Methacrylic Acid) Sample as a Function of Its Neutralization Degree. *Polymer* **1999**, *40*, 1637−1650.
(62) Pleštil, J.; Ostanevich, Y. M.; Bezzabotnov, V. Y.; Hlavatá, D. Small-Angle Scattering by Polyelectrolyte Solutions. Hydration and Conformation of Poly(Methacrylic Acid). *Polymer* **1986**, *27*, 1241−1246.
(63) Stals, P. J. M.; Gillissen, M. A. J.; Paffen, T. F. E.; De Greef, T. F. A.; Lindner, P.; Meijer, E. W.; Palmans, A. R. A.; Voets, I. K. Folding Polymers with Pendant Hydrogen Bonding Motifs in Water: The Effect of Polymer Length and Concentration on the Shape and Size of Single-Chain Polymeric Nanoparticles. *Macromolecules* **2014**, *47*, 2947−2954.

https://dx.doi.org/10.1021/acs.macromol.0c02341
Macromolecules 2021, 54, 1425−1440

(64) Klein, K.; Simon, J.; Wolf, T.; Mailänder, V.; Wurm, F. R.; Landfester, K. Hydrophilicity Regulates the Stealth Properties of Polyphosphoester-Coated Nanocarriers. *Angew. Chem., Int. Ed.* **2018**, *57*, 5548−5553.
(65) Yildirim, E.; Dakshinamoorthy, D.; Peretic, M. J.; Pasquinelli, M. A.; Mathers, R. T. Synthetic Design of Polyester Electrolytes Guided by Hydrophobicity Calculations. *Macromolecules* **2016**, *49*, 7868−7876.
(66) Richards, J. A.; Savin, D. A.; Magenau, A. J. D.; Mathers, R. T.; Pasquinelli, M. A. Systematic Insights from Medicinal Chemistry To Discern the Nature of Polymer Hydrophobicity. *Macromolecules* **2015**, *48*, 7230−7236.
(67) Foster, J. C.; Varlas, S.; Couturaud, B.; Jones, J. R.; Keogh, R.; Mathers, R. T.; O'Reilly, R. K. Predicting Monomers for Use in Polymerization-Induced Self-Assembly. *Angew. Chem., Int. Ed.* **2018**, *57*, 15733−15737.
(68) Filippov, S. K.; Verbraeken, B.; Konarev, P. V.; Svergun, D. I.; Angelov, B.; Vishnevetskaya, N. S.; Papadakis, C. M.; Rogers, S.; Radulescu, A.; Courtin, T.; et al. Block and Gradient Copoly(2-Oxazoline) Micelles: Strikingly Different on the Inside. *J. Phys. Chem. Lett.* **2017**, *8*, 3800−3804.
(69) Kříž, J.; Kadlec, P.; Tuzar, Z.; Gordeliy, V. I.; Pospíšil, H.; Pleštil, J. SANS Study of Multilayer Nanoparticles Based on Block Copolymer Micelles. *Polymer* **2002**, *42*, 2941−2946.
(70) Hone, J. H. E.; Cosgrove, T.; Saphiannikova, M.; Obey, T. M.; Marshall, J. C.; Crowley, T. L. Structure of Physically Adsorbed Polymer Layers Measured by Small-Angle Neutron Scattering Using Contrast Variation Methods. *Langmuir* **2002**, *18*, 855−864.
(71) Estrela-Lopis, I.; Leporatti, S.; Moya, S.; Brandt, A.; Donath, E.; Möhwald, H. SANS Studies of Polyelectrolyte Multilayers on Colloidal Templates. *Langmuir* **2002**, *18*, 7861−7866.
(72) Eastoe, J.; Brown, P.; Smith, G. N.; Gillespie, D. A. J.; James, C.; Rogers, S. E.; Kemp, R.; Alexander, S.; Heenan, R. K.; Grillo, I. Interaction between Surfactants and Colloidal Latexes in Nonpolar Solvents Studied Using Contrast-Variation Small-Angle Neutron Scattering. *Langmuir* **2014**, *30*, 3422−3431.
(73) Kaler, E. W.; Wagner, N. J.; Nettesheim, F.; Liberatore, M. W.; Vethamuthu, M.; Hodgdon, T. K. Influence of Nanoparticle Addition on the Properties of Wormlike Micellar Solutions. *Langmuir* **2008**, *24*, 7718−7726.
(74) Haraguchi, K.; Okabe, S.; Takehisa, T.; Miyazaki, S.; Karino, T.; Shibayama, M. Small-Angle Neutron Scattering Study on Uniaxially Stretched Poly(N -Isopropylacrylamide)−Clay Nanocomposite Gels. *Macromolecules* **2005**, *38*, 10772−10781.
(75) Nusser, K.; Neueder, S.; Schneider, G. J.; Meyer, M.; Pyckhout-Hintzen, W.; Willner, L.; Radulescu, A.; Richter, D. Conformations of Silica-Poly (Ethylene-Propylene) Nanocomposites. *Macromolecules* **2010**, *43*, 9837−9847.
(76) Breßler, I.; Kohlbrecher, J.; Thünemann, A. F. SASfit: A Tool for Small-Angle Scattering Data Analysis Using a Library of Analytical Expressions. *J. Appl. Crystallogr.* **2015**, *48*, 1587−1598.

https://dx.doi.org/10.1021/acs.macromol.0c02341
Macromolecules 2021, 54, 1425−1440